Journal Pre-proof

Ratiometric and colorimetric fluorescent probe for hypochlorite monitor and application for bioimaging in living cells, bacteria and zebrafish

Xiaojun He, Hong Chen, Chuchu Xu, Jinyi Fan, Wei Xu, Yahui Li, Hui Deng, Jianliang Shen

PII: S0304-3894(20)30015-7

DOI: https://doi.org/10.1016/j.jhazmat.2020.122029

Reference: HAZMAT 122029

To appear in: *Journal of Hazardous Materials*

Received Date: 27 October 2019

Revised Date: 14 December 2019

Accepted Date: 4 January 2020

Please cite this article as: He X, Chen H, Xu C, Fan J, Xu W, Li Y, Deng H, Shen J, Ratiometric and colorimetric fluorescent probe for hypochlorite monitor and application for bioimaging in living cells, bacteria and zebrafish, *Journal of Hazardous Materials* (2020), doi: https://doi.org/10.1016/j.jhazmat.2020.122029

Ratiometric and colorimetric fluorescent probe for hypochlorite monitor and application for bioimaging in living cells, bacteria and zebrafish

Xiaojun He,[a,§] Hong Chen,[c,§] Chuchu Xu,[d] Jinyi Fan,[d] Wei Xu,[a] Yahui Li,[b] Hui Deng[d,*] and Jianliang Shen[a,b,*]

[a]School of Ophthalmology & Optometry, School of Biomedical Engineering, Wenzhou Medical University, Wenzhou, Zhejiang 325035, China

[b]Wenzhou Institute, University of Chinese Academy of Sciences, Wenzhou, Zhejiang 325001, China

[c]Luoyang Key Laboratory of Organic Functional Molecules, College of Food and Drug, Luoyang Normal University, Luoyang, 471934, China

[d]School of Stomatology, Wenzhou Medical University, Wenzhou, Zhejiang 325035, China

[§]These authors contributed equally to this work.

All authors have given approval to the final version of this manuscript.

*Address correspondence to dh0726@163.com (H. Deng); shenjl@wibe.ac.cn (J. Shen)

Graphic abstract

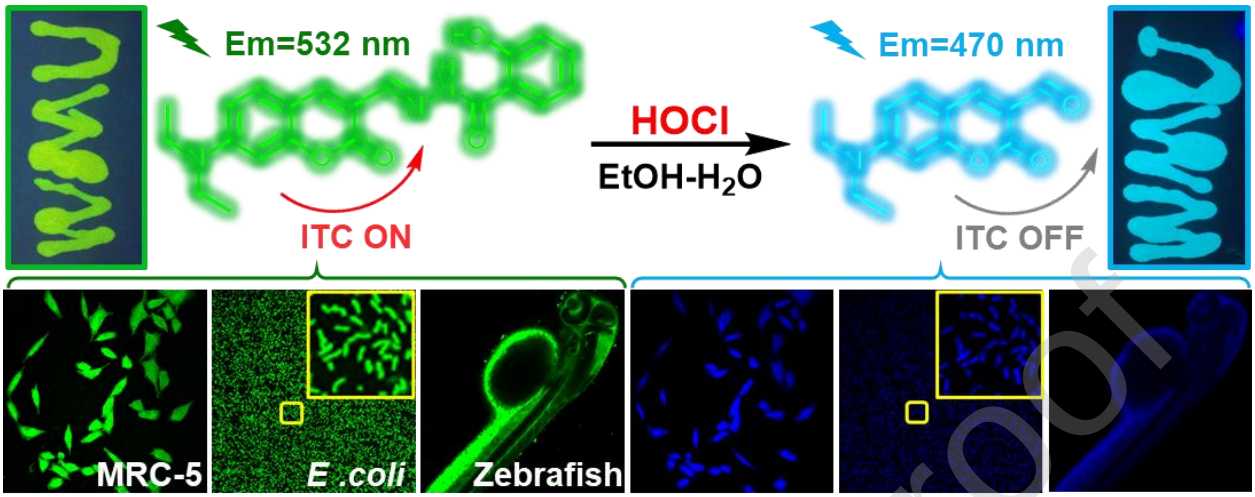

Highlights

- Novelty sensor has employed to sense ClO^- with ratiometric and colorimetric.
- The sensing mechanism was explored by theoretical calculation.
- The chemosensors for ClO^- successful response in cells, bacteria and zebrafish.
- Visualized fluorescence recovery of ClO^- can be realized on filter paper.

Abstract

Hypochlorous acid (HOCl)/hypochlorite (ClO^-) was a biologically important component of reactive oxygen species (ROS) and plays a key role in human immune function systems. HOCl/ClO^- can destroy invasive bacteria and pathogens, and mediate the physiological balance of the organism with low concentrations, and cause oxidation of the biomolecules such as proteins, cholesterol and nucleic acid in biological cells, leading to a series of diseases with over capacity. Therefore, quantifying the content of HOCl/ClO^- in organisms are extremely urgent. In this work, coumarin-salicylic hydrazide Schiff base (**CMSH**), a ratiometric and colorimetric fluorescent probe for ClO^- detection based on coumarin as the fluorophore unit was rationally

designed and synthesized. The results indicated that **CMSH** exhibits high selectivity and sensitivity for ClO^- identification. Additionally, the ratios (I_{470}/I_{532}) displayed brilliant ClO^--dependent quick and sensitive performance within 40 s and limitation of 128 nM, respectively. As well as the color of the solution changes from green to colorless accompanied by the fluorescence form green turns into blue with addition of ClO^-. Totally, **CMSH** has been successfully employed as ratiometric sensor to image in living cells, bacteria and zebrafish with low cytotoxicity and good permeability.

Keywords: Fluorescent probe, Ratiometric and colorimetric, Hypochlorous acid/hypochlorite, Bioimaging in living cells, bacteria and zebrafish

1. Introduction

Reactive oxygen species (ROS), including superoxide radicals, hydroxyl radicals, hydrogen peroxide, singlet oxygen and hypochlorous acid (HOCl)/hypochlorite (ClO^-), play a crucial role in the life system.[1-3] HOCl/ClO^- was one of the important ROS in the body and plays an important role in the human immune function system, which was mainly produced by the reaction of H_2O_2 and Cl^- under catalysis with myeloperoxidase (MPO) in the organism.[4-6] Even if HOCl/ClO^- devotes to the destruction of bacteria in living organisms, and also gives rise to oxidative stress with excessive, and leading to many diseases such as phlegmonosis, angiocardiopathy, atherosclerosis, cancer and kidney diseases.[7-11] However, excessive HOCl/ClO^- can also bring about damage of tissue and a range of complication such as arteriosclerosis, arthritis and cancer, as well as environmental pollution.[12-15] Therefore, it was important to develop an effective method to monitor the changes of HOCl/ClO^- concentration. Fluorescent probes have the advantages of high sensitivity, real-time monitoring and easy operation, and have obvious advantages in detecting analytes in environmental and biological systems.[16, 17] Among them, the organic molecule fluorescent probe has small volume, simple synthesis, fast reaction time, good selectivity, high sensitivity, and fluorescence as an output signal, which was convenient for real-time detection.[18, 19] Hence, small molecule probes were

more and more widely used in environmental detection and chemical analysis, and were widely used in fields such as medicine and biomedicine.[20, 21]

Recently, a number of fluorescent probes capable of specifically identifying ClO^- have been designed and synthesized, including some probes that can be targeted subcellular organelle. Lin et al.[22] developed a ratiometric type fluorescent probe using dehydration reaction of hypochlorous acid for the first time, and the molecular charge was increased due to the large electron pull capability. The transfer process was enhanced, resulting in red shift of the fluorescence spectrum; Yuan et al.[23] designed two-photon hypochlorite probes with naphthalene as the fluorophore, which can locate mitochondria and lysosomes separately; Hu and Zeng et al.[24] based on coumarin and the semi-cyanine dye developed a colorimetric and fluorescent response hypochlorous acid fluorescent probe for the backbone; Wu and Zeng[25] used pyrene as the mother to design and synthesize a ratio of hypochlorous acid fluorescent probe. The introduction of quaternary ammonium salt greatly improved the water solubility of the probe; Nagano et al.[26] adopted the rhodamine located in the mitochondria was a fluorophore, and a fluorescent probe selective for high reactive oxygen species was designed. The photoinduced electron transfer (PET) process in the molecule allows the rhodamine fluorescence to be quenched. However, to date, most of the constructed ClO^- probes were fluorescent enhanced or quenched. Compared with this single emission wavelength change probe, the ratiometric type probe has a dual-wavelength emission characteristic, which was less affected by environmental factors, and has a wide response range, high accuracy, and can realize semi-quantitative analysis, and has been widely used.[27-29] Moreover, the ratiometric probes reported so far have limited their application in organisms due to poor water solubility or their inherent toxicity.

Based on the above characteristics, we have developed a ClO^- ratiometric and colorimetric type fluorescent probe with high selectivity, high sensitivity, good water solubility and low toxicity based on the coumarin parent unit, which can be used for specific rapid detection of aqueous solutions. The probe uses coumarin as the fluorophore to bind salicylate to make it have the overall fluorescence red shift for easy detection. Moreover, the probe has obvious changes in color and fluorescence before and after detection of ClO^-, which could be realized as a dual-function recognition probe with fluorescence and color. It's worth noting that the probe can detect ClO^- in living cells, bacteria and zebrafish, which can effectively achieve imaging results.

2. Experimental section

2.1. Materials and apparatus

All chemicals and solvents were obtained from commercial suppliers with analytical reagents grade. Sodium hypochlorite was purchased from Aladdin stored at 4 ^{o}C, and all of other chemicals were purchased from Aladdin and Sigma-Aldrich. MRC-5 cells were provided by ATCC (Manassas, VA) and zebrafish were got from the Animal Ethics Committee of Wenzhou Medical University. Absorption spectrum and emission spectrum were recorded on UV-2600 form SHIMADZU and RF-45301 from SHIMADZU, respectively. NMR spectra were obtained on a Bruker Ascend 400 spectrometer in DMSO-d_6. LCMS spectra were recorded on the waters zq 2000 spectrometer with HPLC (waters 2695). Cells and zebrafish fluorescent images were acquired on confocal microscopy with Nikon-A1.

*2.2. Synthesis of **CMSH***

Accurately weigh (250 mg, 1.0 mmol) of 7-(diethylamino)-2-oxo-2H-methylene-3-carbaldehyde and dissolve in 15 mL of absolute ethanol. To the above solution was added (150 mg, 1.0 mmol) of 2-hydroxybenzohydrazide and mixed well. After stirring the reaction for 16-18 hours at room temperature, the mixture after the reaction was filtered through a Buchner funnel, and the solid precipitate on the cake was washed with ethanol several times to obtain 330 mg of probe **CMSH**, the solid powder of which was orange.[30] Yield: 84%.; ^{1}H NMR (400 MHz, DMSO) δ 11.90 (s, 2H), 11.85 (s, 1H), 8.43 (s, 1H), 8.31(d, *J* = 7.6 Hz, 1H), 7.82 (d, *J* = 8.9 Hz, 1H), 7.36 (t, *J* = 7.6 Hz, 1H), 6.87 (d, *J* = 8.0 Hz, 1H), 6.70 (d, *J* = 7.5 Hz, 1H), 6.68 (d, *J* = 7.6 Hz, 1H), 6.50 (s, 1H), 3.47 (q, *J* = 6.7 Hz, 4H), 1.14 (t, *J* = 6.7 Hz, 6H); ^{13}C NMR (150 MHz, DMSO) δ 165.35, 161.28, 159.99, 157.12, 152.02, 144.01, 139.50, 131.49, 128.67, 119.32, 117.81, 115.94, 112.69, 110.27, 108.54, 96.87, 45.04, 13.10; LC-MS (ESI+) m/z $[M+1]^{+}$: Calcd for $C_{21}H_{22}N_3O_4$, 379.15, found, 380.00.

2.3. Spectrum Measurements

The stock solution of **CMSH** was prepared in EtOH with the concentration of 1 mM, which prepared working solution with EtOH/H_2O (v/v, 1:19) system in 10 μM and 5 μM for absorption spectrum and emission spectrum tests, respectively. The detecting ions (ClO^-) and other various interferential analytes stock solutions [ClO^-, O_2^-, Cl^-, NO_2^-, AcO^-, CO_3^{2-}, $^1O_2$, NO, $ONOO^-$, SO_4^{2-}, •OH, $S_2O_3^{2-}$, Cys, GSH and H_2O_2] were prepared at 1 mM in deionized water. The work system solution contained **CMSH**, EtOH/H_2O (1:19) and 16 equiv. of each analytes.

2.4. Cytotoxicity Assays

The toxicological evaluation of **CMSH** to MRC-5 cells were employed by traditional methods MTT assays.[31] MRC-5 cells were cultured and seeded in 96-well plates with 2×10^4 cells/mL, and after treatment by various concentrations of **CMSH** from 0 μM to 80 μM at 37 ^oC for 24h. After that 10 μL MTT (5 mg/mL) was added to each well, and incubated with 4 h under the same condition, and was added 150 μL DMSO to dissolve precipitation after the supernatants were aspirated. To record the absorbance at 570 nm by microplate reader. The cell viability (%) = (ODs-ODb) / (ODc-ODb) × 100 %, there s-sample, b-blank and c-control.

2.5. Cell Culture and Imaging

Dulbecco's Modified Eagle Medium (DMEM, Hyclone) used for MRC-5 cells cultured, and 10% fetal calf serum (FBS, Sijiqing), penicillin (100 U / ml, Hyclone) and streptomycin sulfate (100 U / ml, Hyclone) were added in above medium, and cultured at 37 ^oC of 5% CO_2 and 95% air atmosphere condition.[32-34] MRC-5 cells were seeded in new confocal dish processing for the night prior to imaging experiments. After that the cells were pretreated with 5 μM free **CMSH** for 20 min, and then incubated with 20 μM, 40 μM and 80 μM of ClO^- for 20 min. Cellular imaging was performed after washing the cells thrice with PBS. Fluorescent imaging was taken in green/blue channels on confocal microscopy with Nikon-A1.

2.6. Fluorescence Imaging in Zebrafish

The 4-day old zebrafish were cultured and transferred to 24-well plate, and 5 μM of free **CMSH** was added for 20 minutes and washed with PBS, and then 20 μM, 40 μM and 80 μM of ClO^- were added respectively, which were incubated with 20 minutes further. The zebrafish were washed and transferred to a new confocal dish for narcosis (3-Aminobenzoic acid ethyl ester methanesulfonate, MS222) and imaging.

2.7. Quantum calculations

All calculations were done in the Gaussian 09 package.[35] Firstly, the density functional theory(DFT) method was used to optimize the geometry of the ground state structure before and after the reaction of **CMSH** with ClO^- at the B3LYP/6-31G* level, and the natural bond orbital (NBD) analysis was performed on the optimized model. Based on the optimized configuration of the ground state, the TD-DFT method was applied to calculate the excited state at the B3LYP/6-311++G** level. Then, the excited state geometry was optimized at the B3LYP/6-31G* level

and the excited state was calculated. In order to investigate the influence of calculation method and solvation effect on the calculation results, we use the continuous polarization medium model (PCM) to complete the geometric structure optimization and the excited state calculation with ethanol and water as the medium. The results show that the geometry optimization after solvent addition was completed. There was no significant difference between the calculation results of the energy levels. Therefore, the calculation results and discussion in this paper do not include the solvent effect.

2.8. Live subject statement

All animal operations (fluorescence imaging in zebrafish) were performed in accordance with the guidelines for laboratory animal care and use at Wenzhou Medical University and approved by the Animal Ethics Committee of Wenzhou Medical University.

3. Results and discussion

3.1 Design and synthesis

Diethylamino-coumarin dye was used as the building basics to assemble fluorescent probe **CMSH** with wonderful photophysical property, such as high fluorescence quantum yield, which were an important indicator of the application of probes in the field of biology. Whereas, absorption and emission spectra of diethylamino-coumarin were restricted at 400 nm -500 nm, which was not only lacks tissue penetration, but also was strongly interfered by the background of its own fluorescence. To push the emission with red shift, we were employed diethylamino-coumarin aldehyde as one building basic, and then modified with salicylhydrazide to form water solubility **CMSH** with specific spectral properties (Scheme 1). The structure of **CMSH** was confirmed by ^{1}H and ^{13}C NMR and MS as shown in Fig.S1-S3. Details of the synthesis steps, structural analysis, etc. were provided in the experimental section and supplementary information. According to existing reports, hypochlorite (ClO^-)/hypochlorous acid (HOCl) have strong affinity to double bonds. It was foreseeable that when the C=N bond was destroyed with oxygenization by ClO^-, the large π conjugate of **CMSH** will be destroyed, which was acted as a colorimetric and ratiometric chemosensor respond to ClO^-. The coumarin–salicylhydrazide sensor displayed emission maximum at 532 nm (Fig. S5). Consequently, with increase of ClO^-, the color of probe solution system from green turn into colourless. Meanwhile, original green

fluorescence from **CMSH** will gradually fade, and the blue fluorescence from coumarin aldehyde building block will rise. It could be seen that **CMSH** will reveal dual colorimetric and proportional fluorescence responses to ClO^-.

*3.2 Ratiometric and colorimetric response of **CMSH** towards ClO^-*

The spectroscopic analysis with **CMSH** to the monitoring of ClO^- was investigated, which were carried out in EtOH/H_2O system at ambient temperature. The probe **CMSH** solution system displayed green color with green fluorescence under the excitation wavelength at 390 nm. With addition of ClO^- (16 equiv.), the green color of **CMSH** instantly turn into colourless, which could be distinguished ClO^- use colorimetric with the naked eye, and the fluorescence from green turn into blue (Fig. 1 inset). To examine the response of **CMSH** to ClO^-, the spectra titrations were performed. As shown in Fig. 1, **CMSH** shows a conspicuous absorption signal at 456 nm and the expected emission signal at 532 nm. With the increase of ClO^- concentration, the fluorescence intensity of **CMSH** at 532 nm regularly attenuated, and a newly blue-shifted emission signal at 470 nm appeared. At the same time, the symbolic absorption signal shifts from 456 nm to 348 nm, indicating that the whole π conjugate of **CMSH** were destroyed with addition of ClO- to 16 equivalents. In addition, the newly formed emission signal reached a ratio of (F_{470}/F_{532}) at 9.2-times, indicating that **CMSH** can be used as a ratiometric chemosensor for ClO-. It is noteworthy that proportional fluorescent probes require a significant proportional signal change at two wavelengths because the dynamic range of the proportional probe are proportionally controlled.

Linear correction was performed between the absorbance ratio (A_{348}/A_{456}) and ClO^-concentration (0-80 μM) of the corresponding coefficients, and the correction coefficient was higher (R^2 = 0.9728) (Fig. 2c), indicating that **CMSH** can be used for quantitative detection of ClO^- concentration. Additionally, a good linear relationship (R^2 = 0.9716) was obtained by plotting the relative fluorescence intensity ratio value (F_{470}/F_{532}) versus ClO^- concentration at a ClO^- concentration of 0 to 80 μM (Fig. 2d). In addition, **CMSH** could be sensed to low concentrations of ClO^- with a detection limit of 128 nM, which was faceoff with previously published ClO^- proportional fluorescent probes (Table S1). The results indicate that **CMSH** could be detected ClO^- with good advantages of sensitivity.

*3.3 Selectivity of **CMSH** toward ClO^-*

Selectivity was one of the crucial indicators for measuring fluorescent probe applications. To evaluate the selectivity for ClO^-, 5 μM **CMSH** was treated to various biologically relevant ROS, including various analytes (80 μM). In Fig. 2a, only with addition of 80 μM ClO^- led to an obvious color and fluorescence variation of **CMSH**, which could be perceived with the naked eye. However, other analytes (O_2^-, Cl^-, NO_2^-, AcO^-, CO_3^{2-}, $^1O_2$, NO, $ONOO^-$, SO_4^{2-}, •OH, $S_2O_3^{2-}$, Cys, GSH and H_2O_2) only given rise to a negligible ratiometric sensing of **CMSH**. To further insight into the selectivity of **CMSH** for ClO^- over other analytes, we compared the fluorescence ratios (F_{470}/F_{532}) differences of **CMSH** for other interferent. As shown in Fig. 2b, this probe responds to ClO^- significantly strong with the fluorescence over than other analytes. The probe exhibited an apparent chromatic aberration from the color of solution and fluorescence sensing to ClO^- on the strength of oxidization on cleavage of C=N group in **CMSH**, which generated a blue shift emissive diethylamino-coumarin aldehyde. Under the visible light and 365nm UV lamp, the green color of **CMSH** solution changed to colorless only in the presence of ClO^- with the fluorescence changes from green to blue, which was well discriminated by 'naked eye' and fluorescence from **CMSH** in presence of other analytes as shown in Fig. 2c. These results display that **CMSH** could be recognition ClO^- with good selectivity over other biological analytes, which have potential applications to detect ClO^- in various biological environment.

*3.4 Time and pH dependent response of **CMSH** toward ClO^-*

Time dependent fluorescence sensing ClO^- with **CMSH** was investigated. As shown in Fig. 3a, with increasing of ClO^- (16 equiv.), the fluorescence intensity (at 470 nm) increased rapidly and arrived in equilibration within 40 s, which illustrated that **CMSH** could be employed as a "fast sensing" chemosensor for ClO^- and has a potential application to realize for visualized ClO^- in living systems with real-time detection. Furthermore, to evaluate the feasibility of **CMSH** as a multifunctional sensor for ClO^- in different environment conditions, pH-dependent fluorescence sensing to ClO^- was exposed in EtOH/H_2O (v/v = 1/19) with various pH values. In Fig. 3b, the fluorescence intensity ratios (F_{470}/F_{532}) of **CMSH** was unchanged as motionless as a statue from pH 2.0 to 12.0. With present of ClO^- (16 equiv.), the fluorescence intensity of **CMSH** maintain significantly at the pH values undulating from 2.0 to 8.0, which was similar to the p*K*a of ClO^- (p*K*a = 7.53).[36, 37] Hence, **CMSH** can used to detect ClO^- at physiological pH values.

3.5 Proposed sensing mechanism

To confirm the response mechanism of **CMSH** for detecting ClO^-, the reaction product of **CMSH** with ClO^- was were characterized by LC-MS. The probe **CMSH** structure has a very good conjugated system and exhibits strong green fluorescence (532 nm). With addition of sodium hypochlorite, the original conjugated system of the probe was destroyed due to the oxidation of hypochlorite (Fig. 4a). This results in a decrease in fluorescence at Em=532 nm and an increase in fluorescence at Em=470 nm. In order to verify the above conjecture, mass spectrometry was performed on the probe **CMSH** solution to which sodium hypochlorite solution was added. Mass spectrometry showed that the signal peak of m/z=246.0 appeared in the reaction solution, and the mass spectrum signal peak of the probe **CMSH** was [M+H] = 380.0 (Fig. S4). This indicates that the probe **CMSH** was oxidized in the action of hypochlorous acid with the C=N bond was broken, and the original product coumarin aldehyde molecule [M] = 245.1 was formed. The above results indicate that the probe **CMSH** was oxidized under the action of hypochlorous acid to form coumarin aldehyde, and the original conjugated system was destroyed, thereby generating a change in the fluorescent signal. To further estimate the optical behavior of the probes **CMSH** and ClO^- before and after the oxidation reaction, we calculated the optimal geometry of the probe from the B3LYP/6-31G(d) level using density functional theory (DFT) based on the Gaussian 09 program. As shown in Fig. 4b, the highest occupied orbit (HOMO) of the probe **CMSH** was mainly distributed on the salicylhydrazone moiety, and the lowest unoccupied orbital (LUMO) was distributed on the coumarin skeleton. However, when **CMSH** was oxidized by ClO^- to form coumarin aldehyde molecule, the HOMO electron cloud of the coumarin aldehyde molecule was uniformly distributed throughout the structure, and the LUMO was biased toward the other end of the molecular skeleton. In addition, after reacting with ClO^-, the HOMO-LUMO level difference of the probe **CMSH** was 0.11558 eV lower than the energy level difference of the probe **CMSH** (0.13416 eV), which causes the Stokes shift to decrease, so that the maximum emission wavelength becomes shorter.

3.6 Cell imaging

Encouraged by the merits results of spectroscopy displayed above, to investigate the potential application of **CMSH** for detection ClO^- in living cells, cell bioimaging were executed in MRC-5 cell lines. Cell cytotoxicity of **CMSH** was performed by MTT assay, and the results displayed that about 80% of cells still remained alive even though 80 μM **CMSH** was normalized for 24 h (Fig. S6), revealing that **CMSH** has low cytotoxicity and could be further used for cell imaging

experiments. Subsequently, to demonstrate the capability of this probe to sense exogenous ClO^- in living cells, we performed imaging assay with control group and treatment group as powerful evidence. As shown in Fig. 5, MRC-5 cells presented a clear cell profile with green fluorescence in green channel and non-fluorescence in blue channel after incubation with 5 μM **CMSH** for 20 min. Additionally, the MRC-5 cells were incubation with 5 μM **CMSH**, and further treatment with 20 μM, 40 μM and 80 μM ClO^- for 20 min respectively, which the green fluorescence was faded away and blue fluorescence increasingly prominent. As the concentration of ClO^- increased, the blue fluorescence from MRC-5 cells became much stronger and the original green fluorescence gradually faded away. The ratio images (F_{blue}/F_{green}) (Fig.5d, 5h, 5l and 5q) were recorded by mediating the blue channel images (Fig. 5b, 5f, 5j and 5o) with the green channel images (Fig. 5c, 5g, 5k and 5p), which was prominent movement for blue channel after the addition of ClO^-. Cells treated with coumarin (5 μM) as a control group, and found that the cells imaged blue fluorescence, and the cells still imaged blue fluorescence after treatment with 80 μM ClO^- (Fig. S7). Cell imaging results revealed that **CMSH** has good cell permeability and could be act as a ratiometric fluorescence imaging of ClO^- in living cells.

3.7 Bacteria imaging

Reactive oxygen species (ROS) was closely related to the aerobic metabolism and the formation of enzyme in bacteria, and the enzyme-catalyzed reaction was mainly carried out on the cell membrane. Therefore, the production of ROS was focused on the membrane of bacteria.[38-40] Recently, It has been reported that ROS has a direct relationship with the growth of bacteria, and it has great significance to explore the content of ROS in bacteria for the development of new antibacterial drugs, clinical medicine, and food safety. Hence, fluorescence monitor of ROS (ClO^-) in bacteria would be useful to get insight into this antimicrobial mechanism. However, there was little research on imaging in bacteria at present, which was required for the sensor to have powerful fluorescence intensity, stability and permeability. To explore its application further, **CMSH** were employed to sense ClO^- in *E. coli* via bioimaging using fluorescence imaging. As illustrated in Fig. 6, the *E. coli* stained by 5 μM **CMSH** alone showed an obvious fluorescence in the green channel in *E. coli* and no fluorescence the blue channel. With the addition of 20 μM, 40 μM and 80 μM ClO^- for 20 min respectively, the fluorescence of *E. coli* in

the green fluorescence was faded away and blue fluorescence increasingly with prominent, and the "rhabditiform" shape of *E. coli* could be clearly visualized from the fluorescent pattern in the zoomed area. The ratiometric images (F_{blue}/F_{green}) (Fig.6d, 6h, 6l and 6q) were recorded by mediating the blue channel images (Fig. 6b, 6f, 6j and 6o) with the green channel images (Fig. 6c, 6g, 6k and 6p), which was prominent movement for blue channel after the addition of ClO^-. *E. coli* treated with coumarin (5 μM) as a control group, and found that *E. coli* imaged blue fluorescence, and *E. coli* still imaged blue fluorescence after treatment with 80 μM ClO^- (Fig. S7). These results proved that **CMSH** could be applied in tracing ClO^- in *E. coli*, which would be a potential tool to study the biotransformation of ClO^- in bacteria.

3.8 Zebrafish imaging

In normal metabolic processes, organs of an organism could spontaneously produce various ROS. So far, the majority of reported studies demonstrated the possibility of fluorescence imaging of ROS either by single fluorescent channel. However, bioimaging ROS by fluorescent probes in normal organisms with multi-fluorescent channel was still limited by the sensitivity and stability of the probe and its ability to pass various biological barriers. Numerous biological processes were produced in the purtenance of living animals, causing ROS (ClO^-) to self-generate there. Therefore, to investigate the potential biological application of **CMSH** responding to ClO^- in a living organism with green and blue fluorescent channel, four-day-old zebrafishes, a popular vertebrate model, were chosen as our research model system. In Fig.7, it showed that when the zebrafish were cultured in embryo medium, and incubated with free probe **CMSH** (5 μM) for 20 min to allow **CMSH** to permeate into the whole tissues of zebrafish, they exhibited a visible green fluorescence in their abdomen area, this results indicated that the probe was able to penetrate in tissues of zebrafish with emitting fluorescence. There was almost no fluorescence found in the blue channel when the zebrafish were pretreated with **CMSH**. In addition, the zebrafish pretreated with **CMSH** and washed thrice with PBS, and further incubated with 20 μM, 40 μM and 80 μM ClO^- for 20 min respectively, displayed a remarkable changed that the green fluorescence was faded away and blue fluorescence was increasingly prominent in the head and abdomen of zebrafish. The ratiometric images (F_{blue}/F_{green}) (Fig.7d, 7h, 7l and 7q) were recorded by mediating the blue channel images (Fig. 7b, 7f, 7j and 7o) with the green channel images (Fig. 7c, 7g, 7k and 7p), which was prominent movement for blue channel after the addition of ClO^-. Zebrafish treated with coumarin (5 μM) as a control group, and found

that zebrafish imaged blue fluorescence, and zebrafish still imaged blue fluorescence after treatment with 80 μM ClO^- (Fig. S7). Thus, these results convincingly indicated that **CMSH** possessed high tissue penetration capacity and could be realized the visualization of ClO^- in zebrafish with ratiometric fluorescence.

3.9 Application of paper-based probe

As mentioned above, **CMSH** exhibited a noticeable colour change from green to colorless and a significant fluorescence change from green to blue in the presence of ClO^-. Thus, we tentatively prepare a colorimetric solution and test paper model for visual detection of ClO^-. **CMSH** (5 μM) was loaded into a vial, and then different concentrations of ClO^- (0 μM, 10 μM, 15 μM, 20 μM, 25 μM, 30 μM, 35 μM, 40 μM, 45 μM, 50 μM, 55 μM, 60 μM, 65 μM, 70 μM, 75 μM and 80 μM) were added and incubated with **CMSH** (5 μM) for 60s. As shown in Fig. 8, the color of **CMSH** solution in vial turned into colorless gradually with the increase of ClO^-, which was recognition with the naked eye (Fig. 8a). Meanwhile, the fluorescence of **CMSH** solution (5 μM) changed from green fluorescence to blue fluorescence under 365 nm UV lamp (Fig. 8b). For practical applications, it is necessary to develop a sensitive, simple, hand-held and cheap paper sensor.[41-43] Herein, **CMSH** act as a ClO^--sensing paper sensor, which could be realized visualizing by fluorescence detection of ClO^-. Firstly, the filter paper was labelled by EtOH/H_2O solution of **CMSH** (5 μM) with 'WMU' pattern, followed by air-drying. And then dropping concentrations of ClO^- (80 μM) on the paper, the sensing signal was recorded under both visible light and UV lamp (365 nm). As shown in Fig. 8e and 8f, with addition of ClO^-, the color of the test paper gradually changed from green to blue under UV lamp (365 nm). Both color and fluorescence of the paper changed under ClO^- with rapid and conspicuous. These results showed that **CMSH** test paper can quickly and conveniently detect ClO^- in an aqueous medium without any spectroscopic instrumentation.

4. Conclusion

In conclusion, we have rationally designed and synthesized **CMSH** as a novel colorimetric and ratiometric chemosensor for ClO^- via the oxidation of fracture the hydrazine into the aldehyde. **CMSH** functions as a HClO-specific fluorescent indicator that features a fast and ultrasensitive response. The detection limit is as low as 128 nM, which is the highest sensitivity achieved to date. Notably, this reaction of the oxidation of fracture the hydrazine into the aldehyde has been

used in fluorescent for ClO^- monitor with rarely reported in previously. Significantly, **CMSH** can be applied to image ClO^- in MRC-5 cells and bacteria for the first time and monitor the concentration-dependent with ratiometric fluorescence. Additionally, the outstanding sensing property and good biocompatibility of **CMSH** in zebrafish revealed that **CMSH** could be successfully applied for ClO^- detection in the organization. Such work on developing colorimetric and ratiometric chemosensors based on ClO^- is ongoing.

Author contribution:

X.H., H.C. and J.S. conceived and designed the experiments; X.H., H.C. and H.D. carried out experiments; H.D. analyzed experimental results; C.X., J.F. and W.X. contributed reagents/materials/analysis tools, and assisted with bioimaging experiments including cells and zebrafish imaging; Y.L. and H.D. performed and analyzed density functional theory calculation; X.H. and J.S. wrote and modified the manuscript.

Declaration of interests

The authors declare that they have no known competing financial interests or personal relationships that could have appeared to influence the work reported in this paper.

The authors declare no competing financial interest.

Acknowledgments

This work was financially supported by the National Natural Science Foundation of China (31800833 and 21977081), Zhejiang Provincial Natural Science of Foundation of China (Z19H180001), the Wenzhou Medical University and Wenzhou Institute of Biomaterials & Engineering (WIBEZD2017001-03).

References

[1] E.T. Chouchani, L. Kazak, M.P. Jedrychowski, G.Z. Lu, B.K. Erickson, J. Szpyt, K.A. Pierce, D. Laznik-Bogoslavski, R. Vetrivelan, C.B. Clish, Mitochondrial ROS regulate thermogenic energy expenditure and sulfenylation of UCP1, Nature, 532 (2016) 112.
[2] S. Di Meo, S. Iossa, P. Venditti, Skeletal muscle insulin resistance: role of mitochondria and other ROS sources, Journal of Endocrinology, 233 (2017) R15-R42.
[3] Z. Liang, T.H. Tsoi, C.F. Chan, L. Dai, Y. Wu, G. Du, L. Zhu, C.S. Lee, W.T. Wong, G.L. Law, K.L. Wong, A smart "off-on" gate for the in situ detection of hydrogen sulphide with Cu(ii)-assisted europium emission, Chem Sci, 7 (2016) 2151-2156.
[4] D. Vara, G. Pula, Reactive oxygen species: physiological roles in the regulation of vascular cells, Current molecular medicine, 14 (2014) 1103-1125.
[5] G. Wang, Chloride flux in phagocytes, Immunological reviews, 273 (2016) 219-231.
[6] A. Strzepa, K.A. Pritchard, B.N. Dittel, Myeloperoxidase: A new player in autoimmunity, Cellular immunology, 317 (2017) 1-8.
[7] C.L.-L. Chiang, L.E. Kandalaft, J. Tanyi, A.R. Hagemann, G.T. Motz, N. Svoronos, K. Montone, G.M. Mantia-Smaldone, L. Smith, H.L. Nisenbaum, A dendritic cell vaccine pulsed with autologous hypochlorous acid-oxidized ovarian cancer lysate primes effective broad antitumor immunity: from bench to bedside, Clinical cancer research, 19 (2013) 4801-4815.
[8] T. Fukuyama, B. Martel, K. Linder, S. Ehling, J. Ganchingco, W. Bäumer, Hypochlorous acid is antipruritic and anti‐inflammatory in a mouse model of atopic dermatitis, Clinical & Experimental Allergy, 48 (2018) 78-88.
[9] M. Boncler, B. Kehrel, R. Szewczyk, E. Stec-Martyna, R. Bednarek, M. Brodde, C. Watala, Oxidation of C-reactive protein by hypochlorous acid leads to the formation of potent platelet activator, International journal of biological macromolecules, 107 (2018) 2701-2714.
[10] R. Jeelani, D. Maitra, C. Chatzicharalampous, S. Najeemuddin, R.T. Morris, H.M. Abu‐Soud, Melatonin prevents hypochlorous acid‐mediated cyanocobalamin destruction and cyanogen chloride generation, Journal of pineal research, 64 (2018) e12463.
[11] I.Q. Tantry, S. Waris, S. Habib, R.H. Khan, R. Mahmood, A. Ali, Hypochlorous acid induced structural and conformational modifications in human DNA: A multi-spectroscopic study, International journal of biological macromolecules, 106 (2018) 551-558.
[12] H. Lin, B.S. Levison, J.A. Buffa, Y. Huang, X. Fu, Z. Wang, V. Gogonea, J.A. DiDonato, S.L. Hazen, Myeloperoxidase-mediated protein lysine oxidation generates 2-aminoadipic acid and lysine nitrile in vivo, Free Radical Biology and Medicine, 104 (2017) 20-31.
[13] H. Feng, Z. Zhang, Q. Meng, H. Jia, Y. Wang, R. Zhang, Rapid Response Fluorescence Probe Enabled In Vivo Diagnosis and Assessing Treatment Response of Hypochlorous Acid‐Mediated Rheumatoid Arthritis, Advanced Science, 5 (2018) 1800397.
[14] J. Marcinkiewicz, E. Kontny, Taurine and inflammatory diseases, Amino acids, 46 (2014) 7-20.
[15] E.O. Santos, L.M. Kabeya, A.S. Figueiredo-Rinhel, L.F. Marchi, M.F. Andrade, F. Piatesi, A.B. Paoliello-Paschoalato, A.E.C. Azzolini, Y.M. Lucisano-Valim, Flavonols modulate the effector functions of healthy individuals' immune complex-stimulated neutrophils: A therapeutic perspective for rheumatoid arthritis, International immunopharmacology, 21 (2014) 102-111.

[16] X. He, C. Wu, Y. Qian, Y. Li, F. Ding, Z. Zhou, J. Shen, Symmetrical bis-salophen probe serves as a selectively and sensitively fluorescent switch of gallium ions in living cells and zebrafish, Talanta, 205 (2019) 120118.
[17] S. Feng, D. Liu, W. Feng, G. Feng, Allyl fluorescein ethers as promising fluorescent probes for carbon monoxide imaging in living cells, Analytical chemistry, 89 (2017) 3754-3760.
[18] B. Yun, K. Roberts, P. Thompson, R. Nation, T. Velkov, J. Li, Design and Evaluation of Novel Polymyxin Fluorescent Probes, Sensors, 17 (2017) 2598.
[19] S. Xu, H.-W. Liu, X. Yin, L. Yuan, S.-Y. Huan, X.-B. Zhang, A cell membrane-anchored fluorescent probe for monitoring carbon monoxide release from living cells, Chemical science, 10 (2019) 320-325.
[20] S. Sun, K.M. Błażewska, A.P. Kadina, B.A. Kashemirov, X. Duan, J.T. Triffitt, J.E. Dunford, R.G.G. Russell, F.H. Ebetino, A.J. Roelofs, Fluorescent bisphosphonate and carboxyphosphonate probes: a versatile imaging toolkit for applications in bone biology and biomedicine, Bioconjugate chemistry, 27 (2015) 329-340.
[21] J. Zhang, K.L. Wong, W.K. Wong, N.K. Mak, D.W. Kwong, H.L. Tam, Two-photon induced luminescence, singlet oxygen generation, cellular uptake and photocytotoxic properties of amphiphilic Ru(II) polypyridyl-porphyrin conjugates as potential bifunctional photodynamic therapeutic agents, Organic & biomolecular chemistry, 9 (2011) 6004-6010.
[22] W. Lin, L. Long, B. Chen, W. Tan, A ratiometric fluorescent probe for hypochlorite based on a deoximation reaction, Chemistry–A European Journal, 15 (2009) 2305-2309.
[23] Z. Ye, R. Zhang, B. Song, Z. Dai, D. Jin, E.M. Goldys, J. Yuan, Development of a functional ruthenium (II) complex for probing hypochlorous acid in living cells, Dalton Transactions, 43 (2014) 8414-8420.
[24] J. Zha, B. Fu, C. Qin, L. Zeng, X. Hu, A ratiometric fluorescent probe for rapid and sensitive visualization of hypochlorite in living cells, RSC Advances, 4 (2014) 43110-43113.
[25] Y. Wu, J. Wang, F. Zeng, S. Huang, J. Huang, H. Xie, C. Yu, S. Wu, Pyrene derivative emitting red or near-infrared light with monomer/excimer conversion and its application to ratiometric detection of hypochlorite, ACS applied materials & interfaces, 8 (2016) 1511-1519.
[26] Y. Koide, Y. Urano, S. Kenmoku, H. Kojima, T. Nagano, Design and synthesis of fluorescent probes for selective detection of highly reactive oxygen species in mitochondria of living cells, Journal of the American Chemical Society, 129 (2007) 10324-10325.
[27] Y. Cai, J. Zhan, H. Shen, D. Mao, S. Ji, R. Liu, B. Yang, D. Kong, L. Wang, Z. Yang, Optimized ratiometric fluorescent probes by peptide self-assembly, Analytical chemistry, 88 (2015) 740-745.
[28] D. Gong, S.-C. Han, A. Iqbal, J. Qian, T. Cao, W. Liu, W. Liu, W. Qin, H. Guo, Fast and selective two-stage ratiometric fluorescent probes for imaging of glutathione in living cells, Analytical chemistry, 89 (2017) 13112-13119.
[29] S. Xia, M. Fang, J. Wang, J. Bi, W. Mazi, Y. Zhang, R.L. Luck, H. Liu, Near-infrared fluorescent probes with BODIPY donors and rhodamine and merocyanine acceptors for ratiometric determination of lysosomal pH variance, Sensors and Actuators B: Chemical, 294 (2019) 1-13.

[30] H. Chen, P. Yang, Y. Li, L. Zhang, F. Ding, X. He, J. Shen, Insight into triphenylamine and coumarin serving as copper (II) sensors with "OFF" strategy and for bio-imaging in living cells, Spectrochimica Acta Part A: Molecular and Biomolecular Spectroscopy, 224 (2020) 117384.
[31] D. Mukhtar-Fayyad, Cytocompatibility of new bioceramic-based materials on human fibroblast cells (MRC-5), Oral Surgery, Oral Medicine, Oral Pathology, Oral Radiology, and Endodontology, 112 (2011) e137-e142.
[32] M. Radu, M. Cristina Munteanu, S. Petrache, A. Iren Serban, D. Dinu, A. Hermenean, C. Sima, A. Dinischiotu, Depletion of intracellular glutathione and increased lipid peroxidation mediate cytotoxicity of hematite nanoparticles in MRC-5 cells, Acta Biochimica Polonica, 57 (2010) 355.
[33] S.M. Ding, A.L. Lu, W. Zhang, L. Zhou, H.Y. Xie, S.S. Zheng, Q.Y. Li, The role of cancer-associated fibroblast MRC-5 in pancreatic cancer, Journal of Cancer, 9 (2018) 614-628.
[34] R. Pan, Y. Zhang, M. Zheng, B. Zang, M. Jin, Hydroxysafflor Yellow A Suppresses MRC-5 Cell Activation Induced by TGF-beta1 by Blocking TGF-beta1 Binding to TbetaRII, Frontiers in pharmacology, 8 (2017) 264.
[35] X. He, C. Wu, Y. Qian, Y. Li, L. Zhang, F. Ding, H. Chen, J. Shen, Highly sensitive and selective light-up fluorescent probe for monitoring gallium and chromium ions in vitro and in vivo, The Analyst, 144 (2019) 3807-3816.
[36] T. Watanabe, K. Akai, Y. Einaga, The reduction behavior of free chlorine at boron-doped diamond electrodes, Electrochemistry Communications, 70 (2016) 18-22.
[37] C. Liu, X. Jiao, S. He, L. Zhao, X. Zeng, A highly selective and sensitive fluorescent probe for hypochlorous acid and its lysosome-targetable biological applications, Talanta, 174 (2017) 234-242.
[38] H.-L. Su, C.-C. Chou, D.-J. Hung, S.-H. Lin, I.-C. Pao, J.-H. Lin, F.-L. Huang, R.-X. Dong, J.-J. Lin, The disruption of bacterial membrane integrity through ROS generation induced by nanohybrids of silver and clay, Biomaterials, 30 (2009) 5979-5987.
[39] P.V. Escribá, J.M. González‐Ros, F.M. Goñi, P.K. Kinnunen, L. Vigh, L. Sánchez‐Magraner, A.M. Fernández, X. Busquets, I. Horváth, G. Barceló‐Coblijn, Membranes: a meeting point for lipids, proteins and therapies, Journal of cellular and molecular medicine, 12 (2008) 829-875.
[40] O. Handa, Y. Naito, T. Yoshikawa, Helicobacter pylori: a ROS-inducing bacterial species in the stomach, Inflammation Research, 59 (2010) 997-1003.
[41] G. Yang, C. Lee, J. Kim, F. Ren, S.J. Pearton, Flexible graphene-based chemical sensors on paper substrates, Physical Chemistry Chemical Physics, 15 (2013) 1798-1801.
[42] P. Hevesi, S. Wille, G. Pirkl, N. Wehn, P. Lukowicz, Monitoring household activities and user location with a cheap, unobtrusive thermal sensor array, in: Proceedings of the 2014 ACM international joint conference on pervasive and ubiquitous computing, ACM, 2014, pp. 141-145.
[43] J.-H. Kim, S. Mun, H.-U. Ko, G.-Y. Yun, J. Kim, Disposable chemical sensors and biosensors made on cellulose paper, Nanotechnology, 25 (2014) 092001.

Figure/caption:

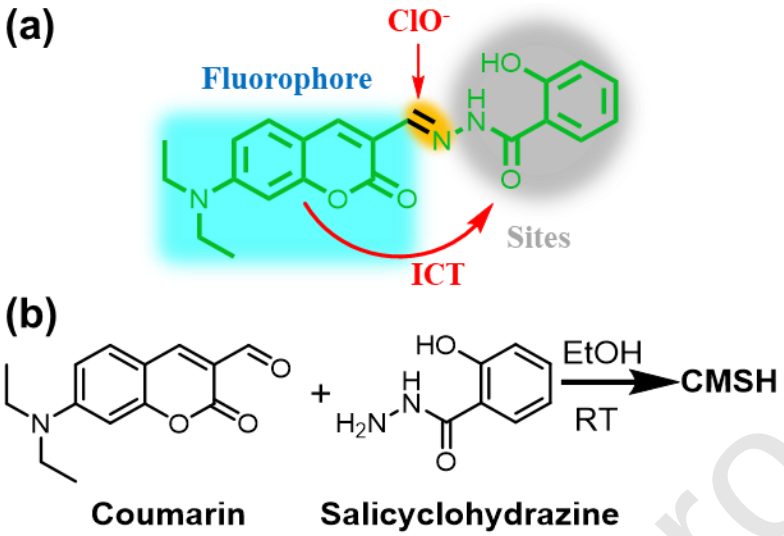

Scheme 1 (a) Design strategy and (b) synthetic route for probe **CMSH**.

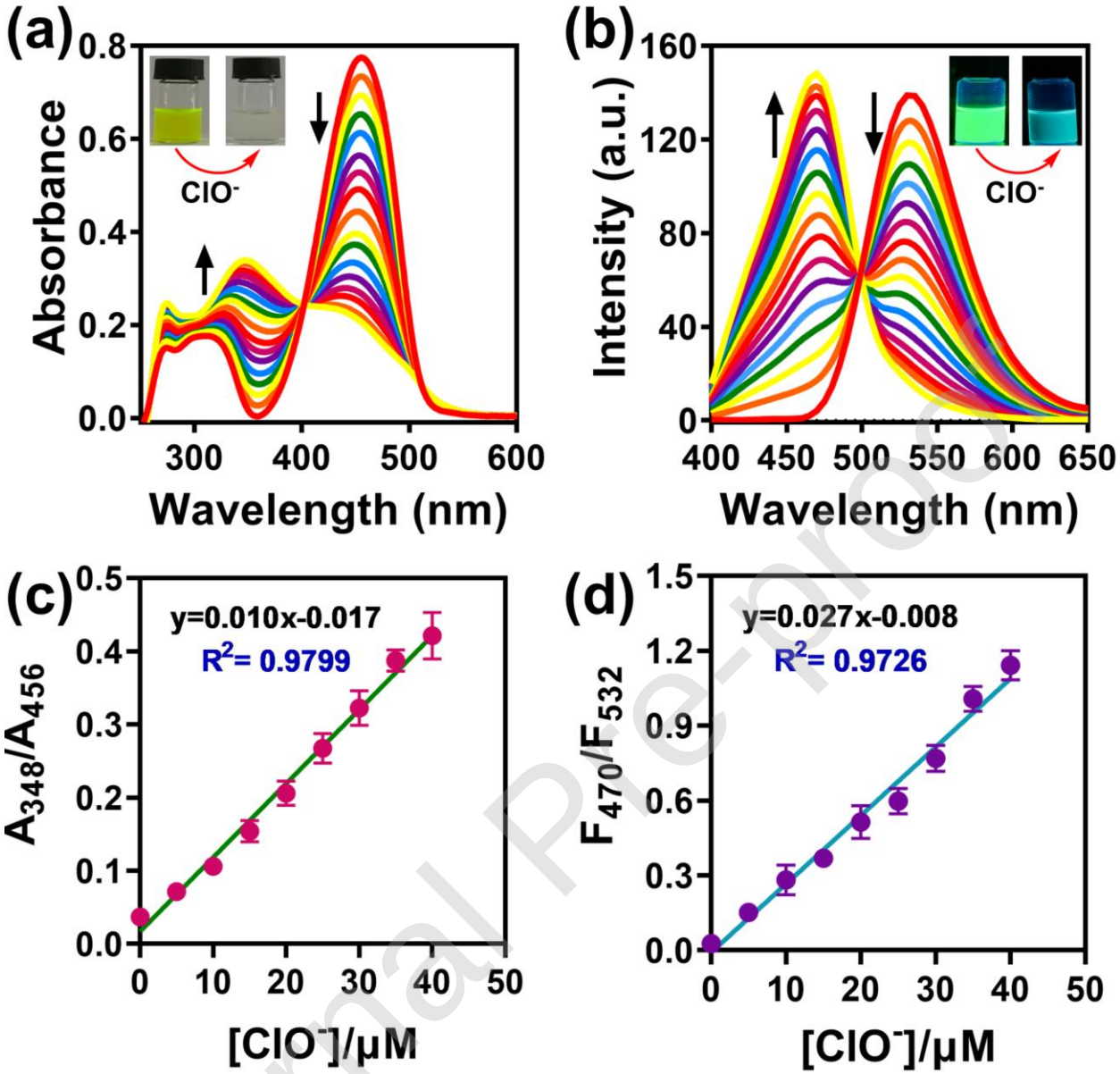

Fig. 1 (a) UV-vis absorption (10 μM) and (b) fluorescence spectra (5 μM) changes of **CMSH** in EtOH/H_2O solution (v/v = 1/19) upon addition of increasing amount of ClO^- (0 – 80 μM). Each spectrum was recorded after 3 min. Inset: (a) The color and (b) fluorescence images of **CMSH** in the absence/presence of ClO^- with 365 nm lamp. Linear relationships between (c) UV-vis absorbance ratios (A_{348}/A_{456}) and (d) fluorescence intensity ratios (F_{470}/F_{532}) of **CMSH** *versus* concentrations of HOCl in EtOH/H_2O solution. R was the correlation coefficient of linear.

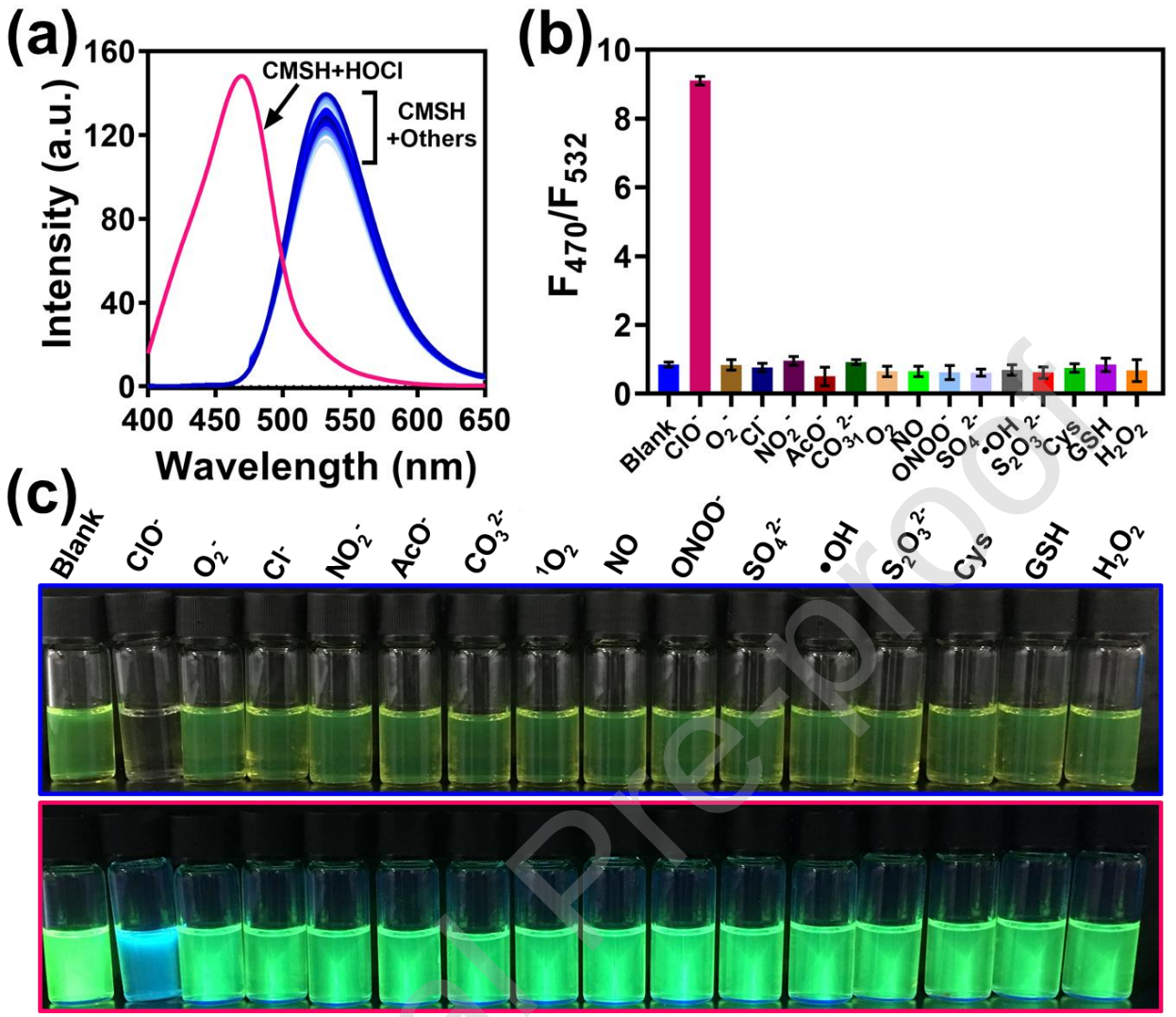

Fig.2 Changes of fluorescence spectra (a), ratio of fluorescence intensity of F_{470}/F_{532} (b), and the fluorescence colour photographs (c) of **CMSH** (5 μM) with various biologically relevant species (80 μM) in EtOH-H_2O (v/v= 1/19): blank, ClO^-, O_2^-, Cl^-, NO_2^-, AcO^-, CO_3^{2-}, $^1O_2$, NO, $ONOO^-$, SO_4^{2-}, •OH, $S_2O_3^{2-}$, Cys, GSH and H_2O_2 with visible and 365 nm lamp.

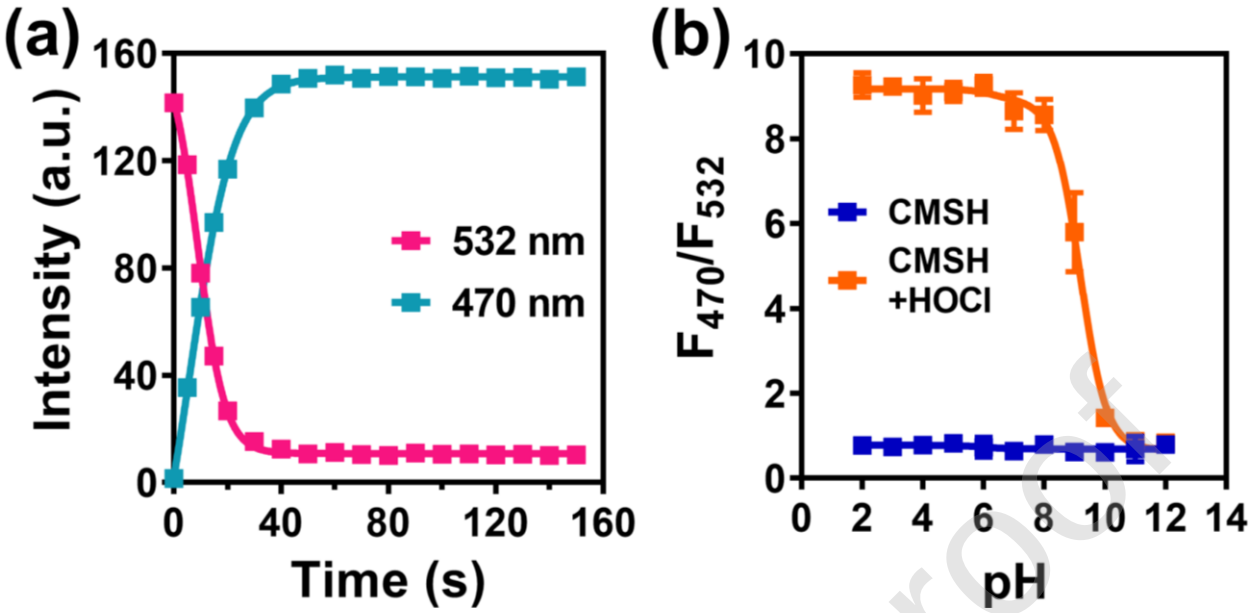

Fig. 3 (a) Time-depend fluorescence responses of 5 μM **CMSH** towards 80 μM ClO^- in EtOH-H_2O solution. (b) Ratiometric fluorescence changes of 5 μM **CMSH** in the absence and presence of 80 μM ClO^- in EtOH-H_2O solution with different pH values. Each spectrum was recorded after 3 min for 3 times.

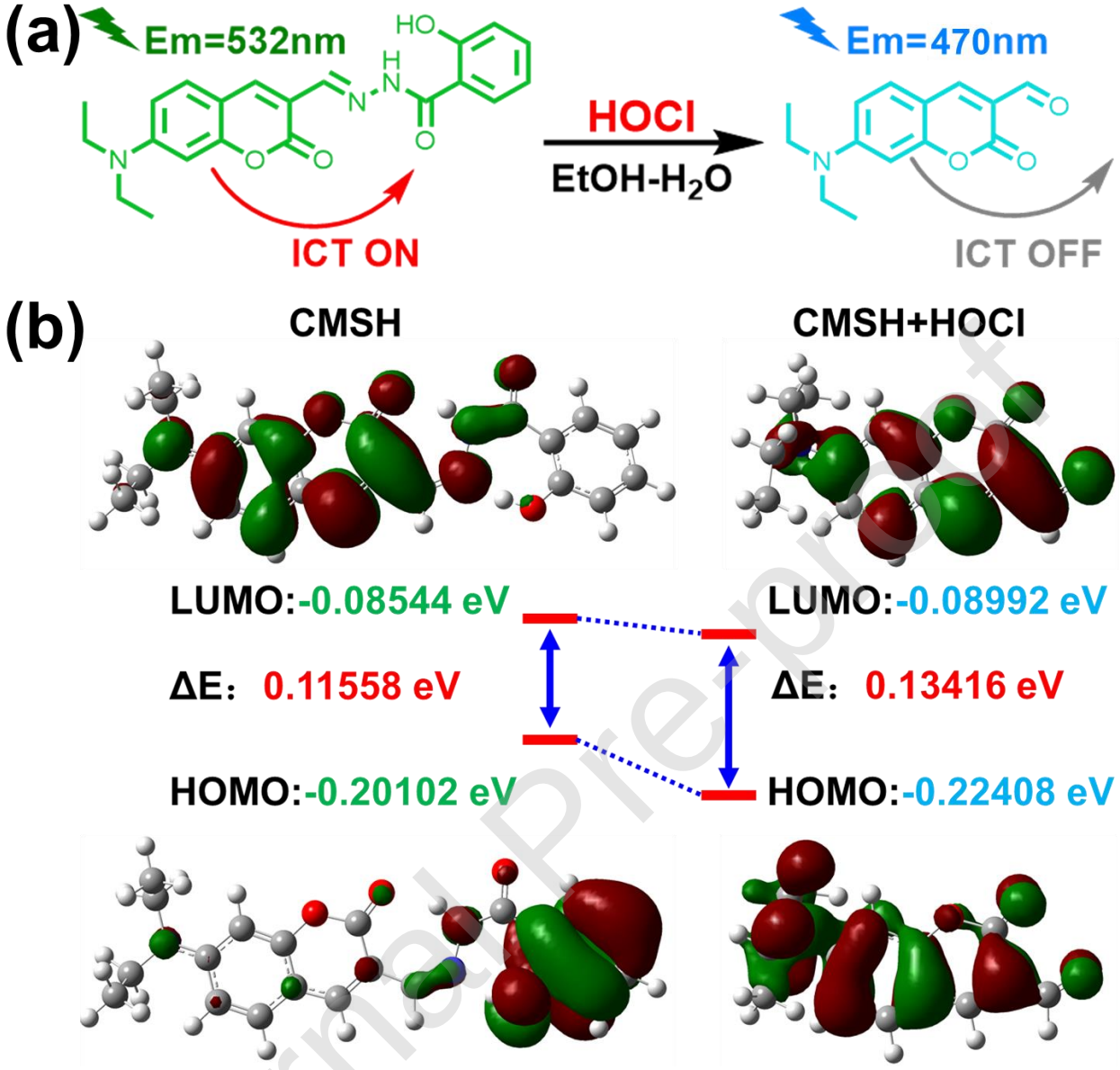

Fig. 4 (a) Proposed mechanism for **CMSH** sensing of ClO^-. (b) HOMO-LUMO energy levels and the interfacial plots of the molecular orbitals for **CMSH** with and without addition of ClO^-.

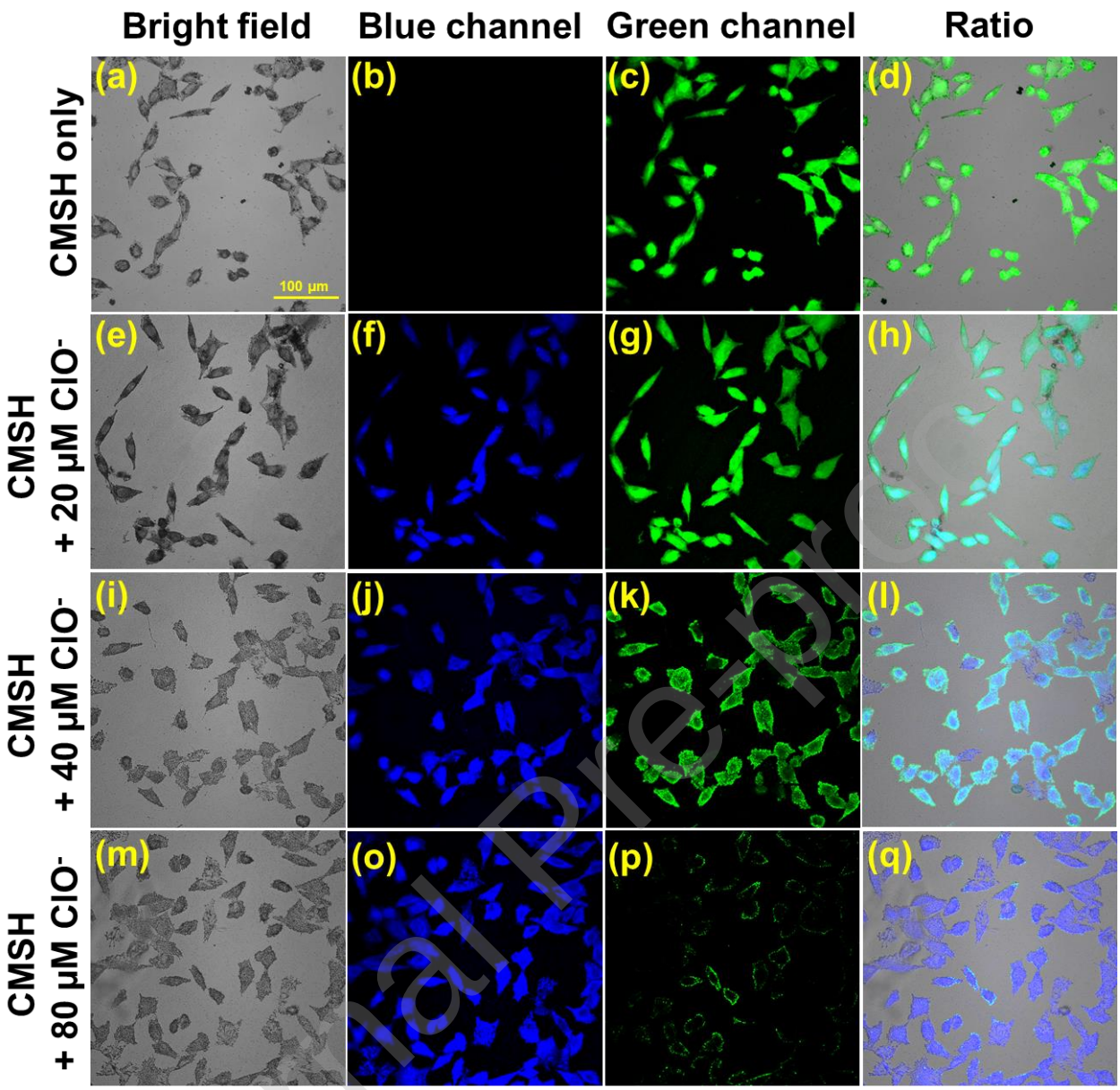

Fig. 5 Relative confocal fluorescence images of MRC-5 cells under different conditions with **CMSH**. MRC-5 cells treated with 5 μM **CMSH** (a-d), then further incubated with 20 μM ClO^- (e-h), 40 μM ClO^- (i-l) and 80 μM ClO^- for 10 min (m-q). Fluorescence images from left to right: blue channel, green channel and ratiometric images (Fblue/Fgreen). Scale bar: 100 μm.

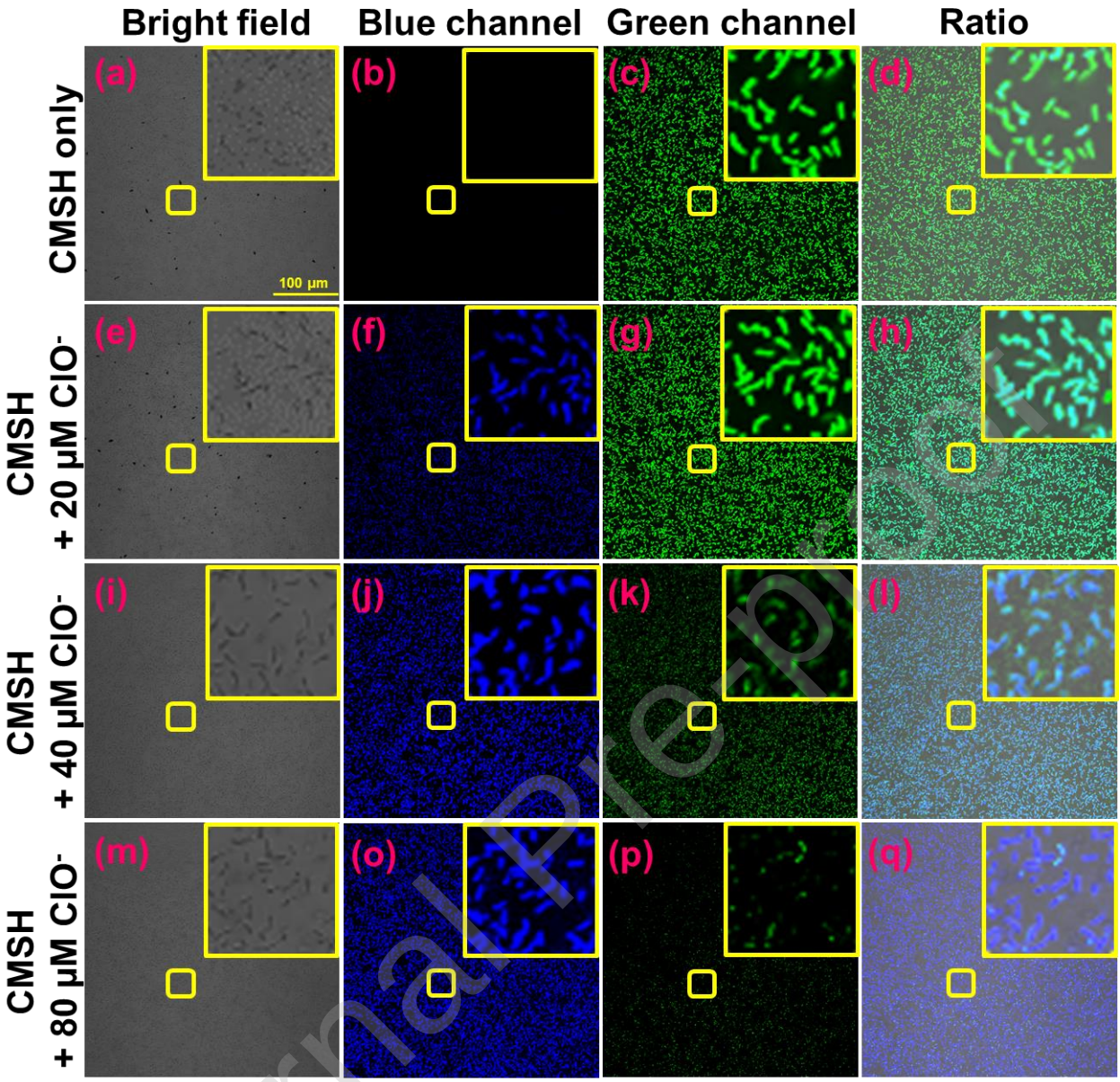

Fig.6 Confocal fluorescence images of *E. coli*. Fluorescent image of *E. coli* stained with **CMSH** (5 μM) for 20 min (a-d). *E. coli* were incubated with **CMSH** for 20 min, further incubated with 20 μM ClO^- (e-h), 40 μM ClO^- (i-l) and 80 μM ClO^- for 10 min (m-q). Insert: local zoom of the photograph.

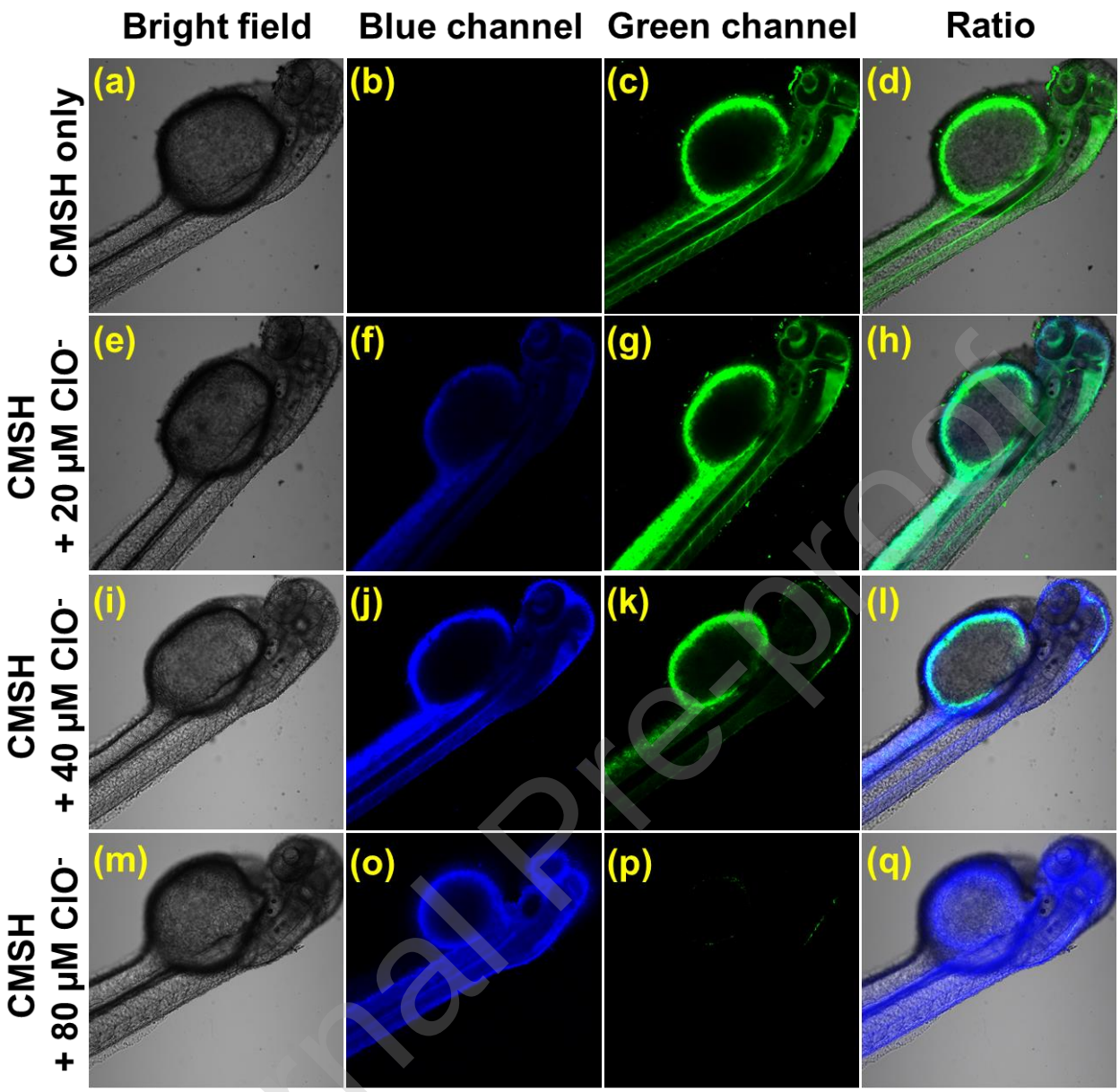

Fig.7 Confocal fluorescence images of zebrafish. Fluorescent image of zebrafish stained with **CMSH** (5 μM) for 20 min (a-d). Zebrafish were incubated with **CMSH** for 20 min, further incubated with 20 μM ClO^- (e-h), 40 μM ClO^- (i-l) and 80 μM ClO^- for 10 min (m-q).

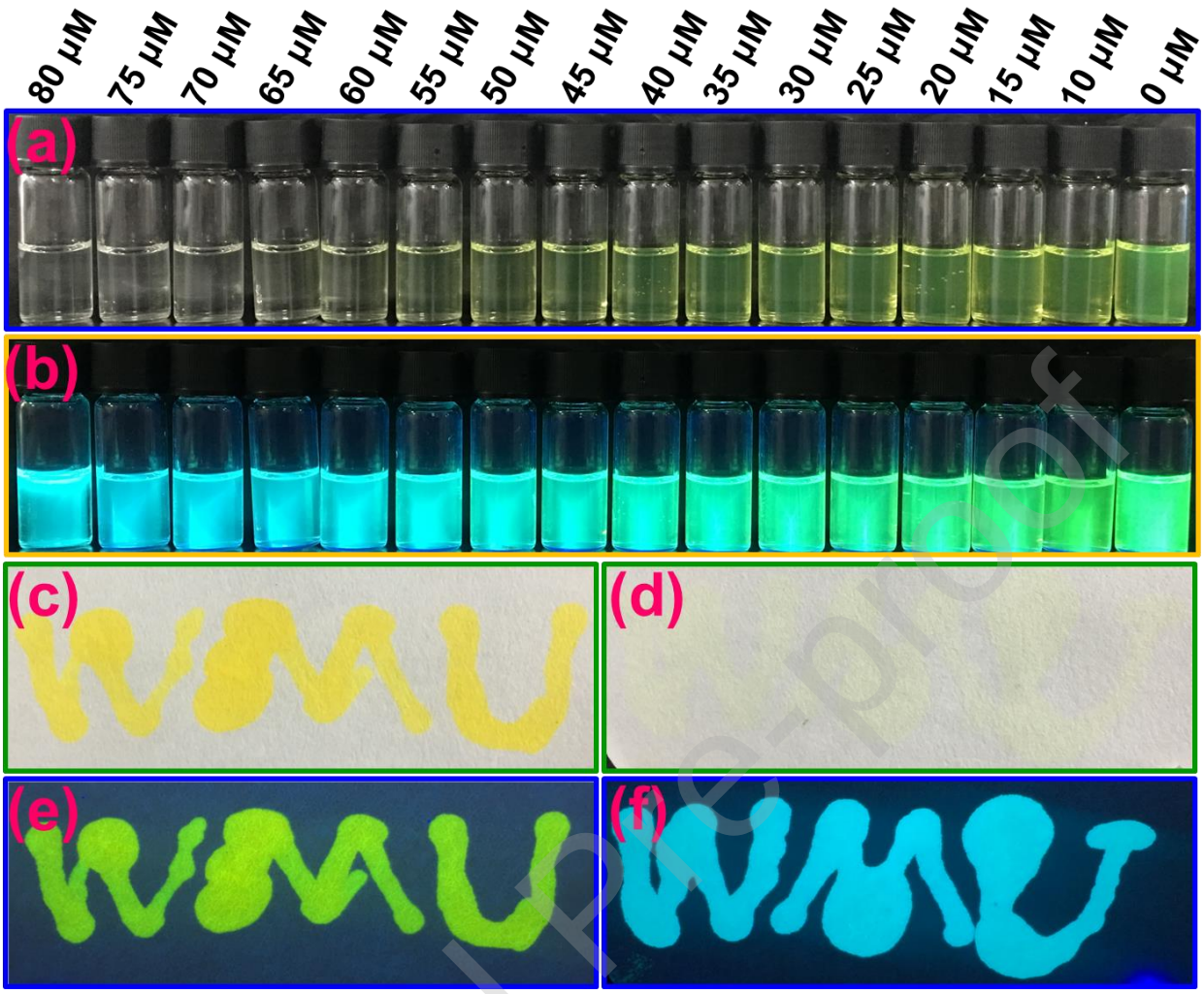

Fig. 8 CMSH (5 μM) as a reagent kit for determination of ClO^-. (a) The color and (b) fluorescence images of **CMSH** reagent (5 μM) in the presence of different concentrations of ClO^-. Photograph of (c, d) color and (e, f) fluorescence of probe **CMSH** (5 μM) test paper in the absent and presence of (80 μM) of ClO^- under a hand-held UV lamp (365 nm).

Supporting Information

Ratiometric and colorimetric fluorescent probe for hypochlorite monitor and application for bioimaging in living cells, bacteria and zebrafish

Xiaojun He,[a,§] Hong Chen,[c,§] Chuchu Xu,[d] Jinyi Fan,[d] Wei Xu,[a] Yahui Li,[b] Hui Deng[d,*] and Jianliang Shen[a,b,*]

[a]School of Ophthalmology & Optometry, School of Biomedical Engineering, Wenzhou Medical University, Wenzhou, Zhejiang 325035, China

[b]Wenzhou Institute, University of Chinese Academy of Sciences, Wenzhou, Zhejiang 325001, China

[c]Luoyang Key Laboratory of Organic Functional Molecules, College of Food and Drug, Luoyang Normal University, Luoyang, 471934, China

[d]School of Stomatology, Wenzhou Medical University, Wenzhou, Zhejiang 325035, China

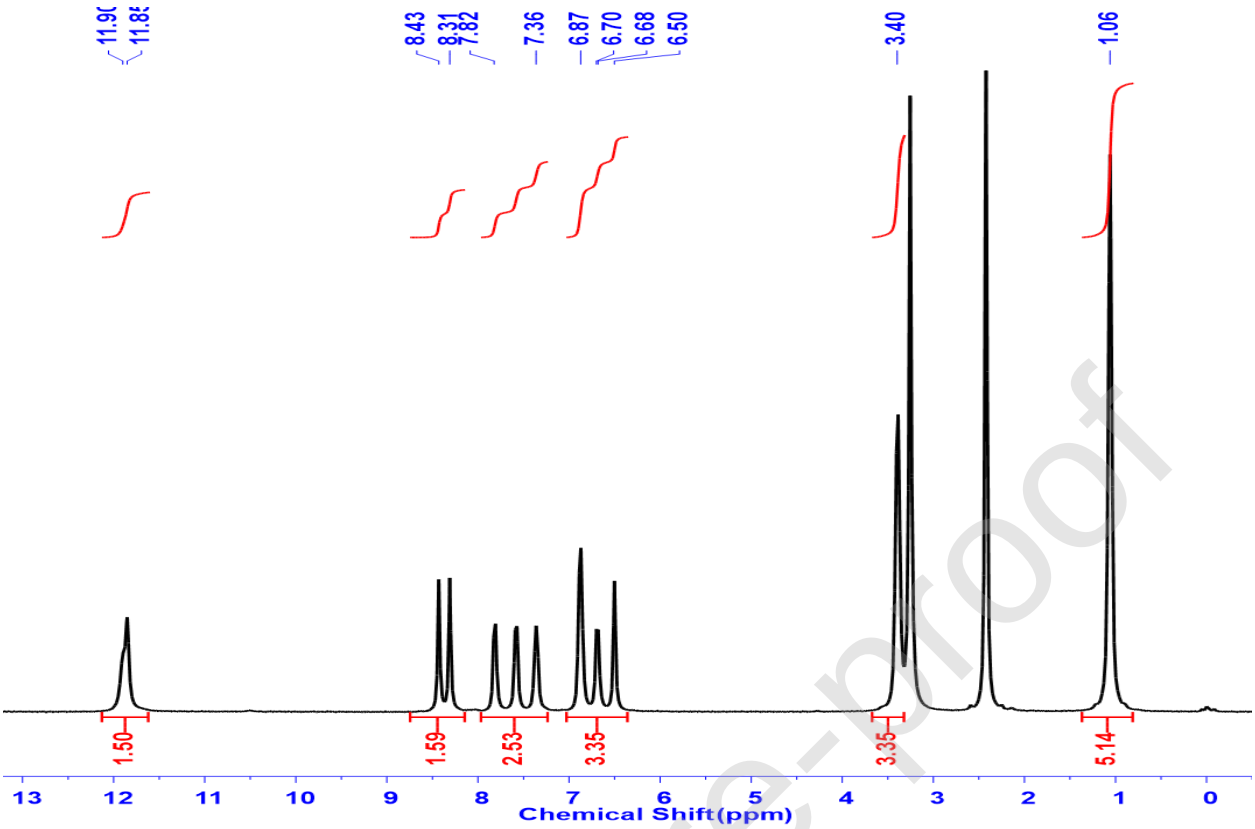

Fig. S1 ^{1}H NMR spectra of **CMSH** in DMSO-*d6*.

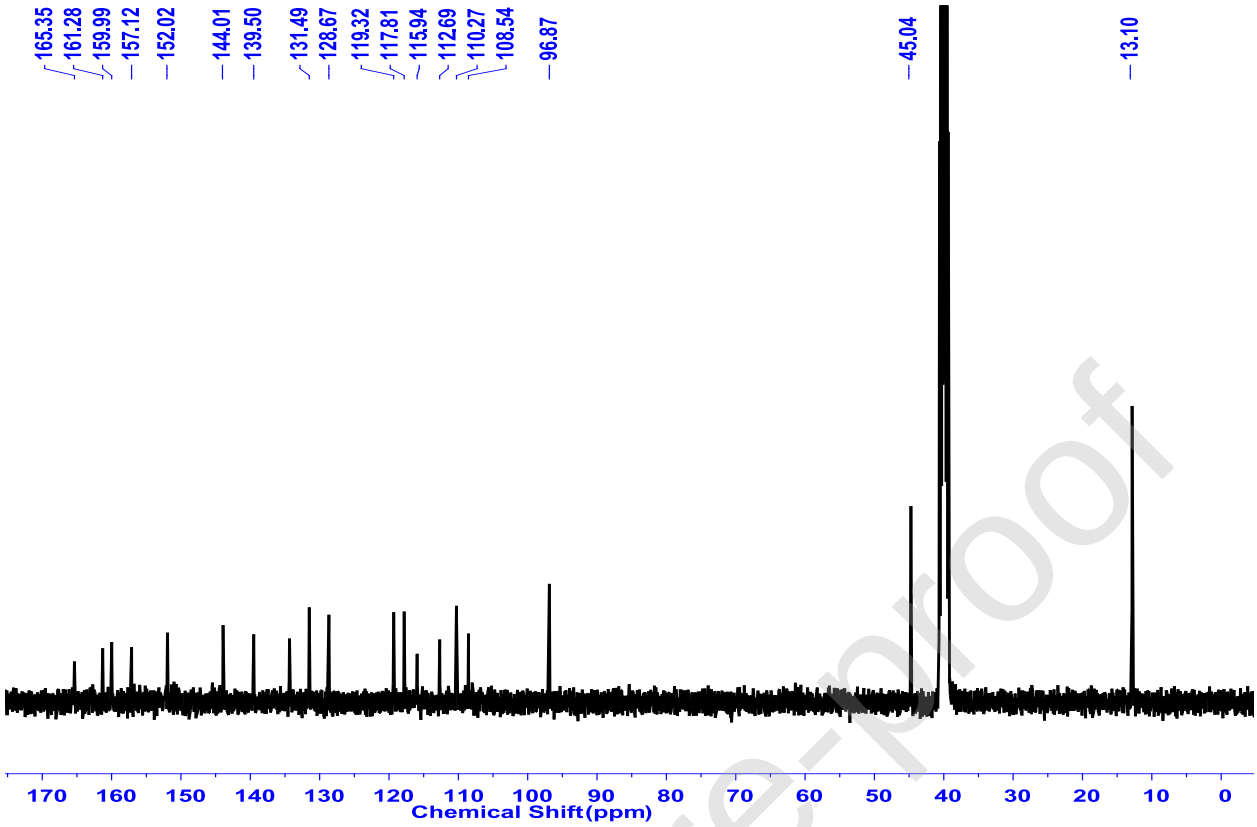

Fig. S2 ^{13}C NMR spectra of **CMSH** in DMSO-*d6*.

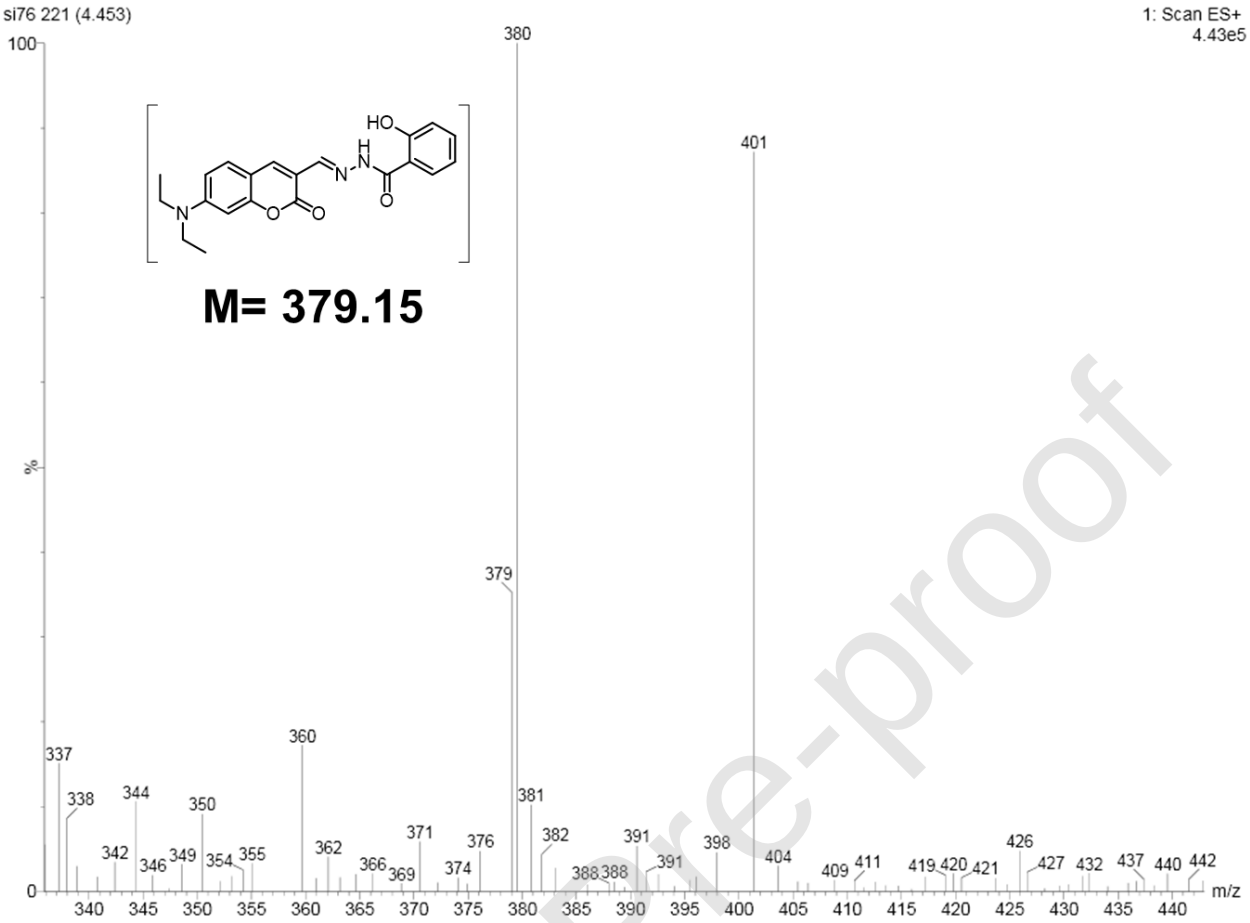

Fig. S3 Mass spectrum of **CMSH** in EtOH.

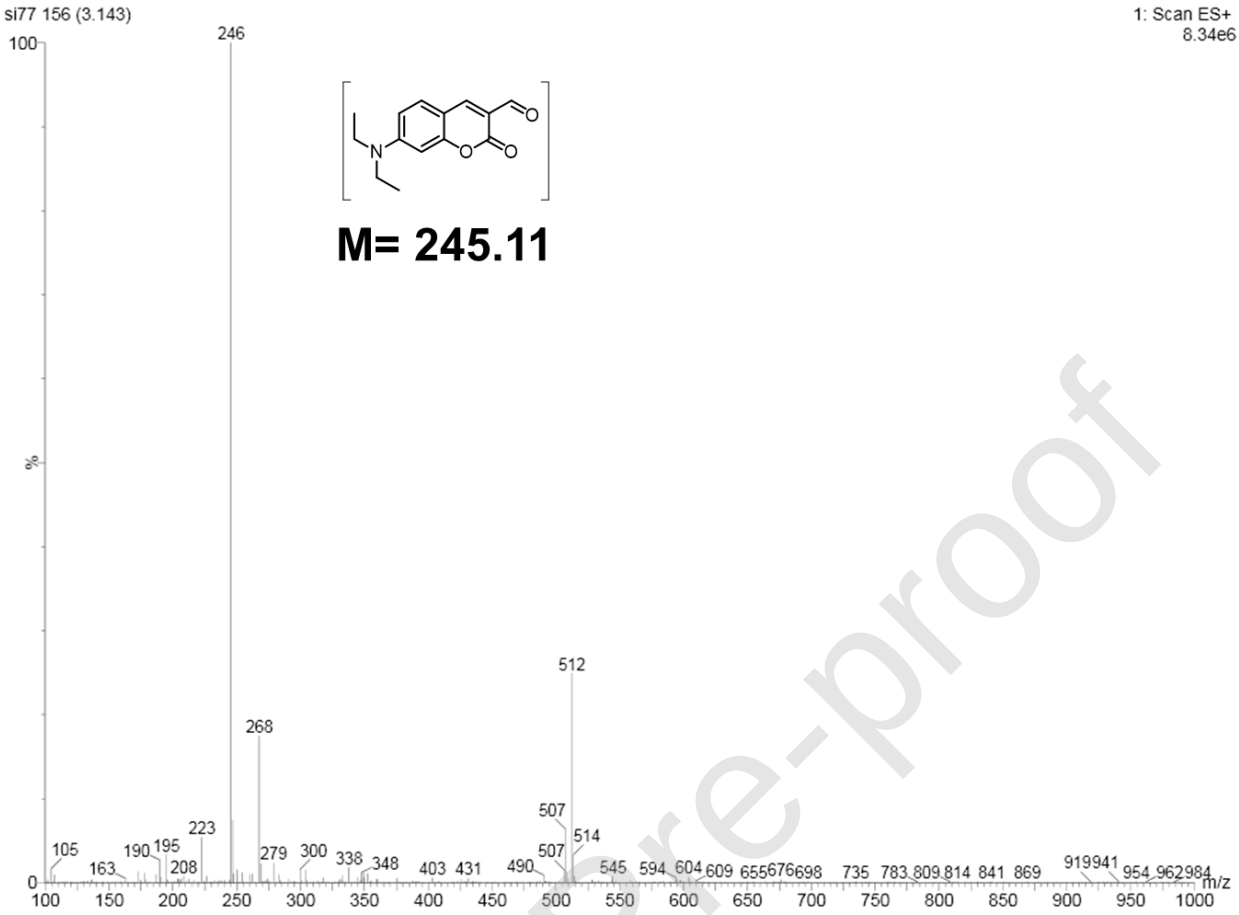

Fig. S4 Mass spectrum of **CMSH** after reaction with ClO^- in EtOH.

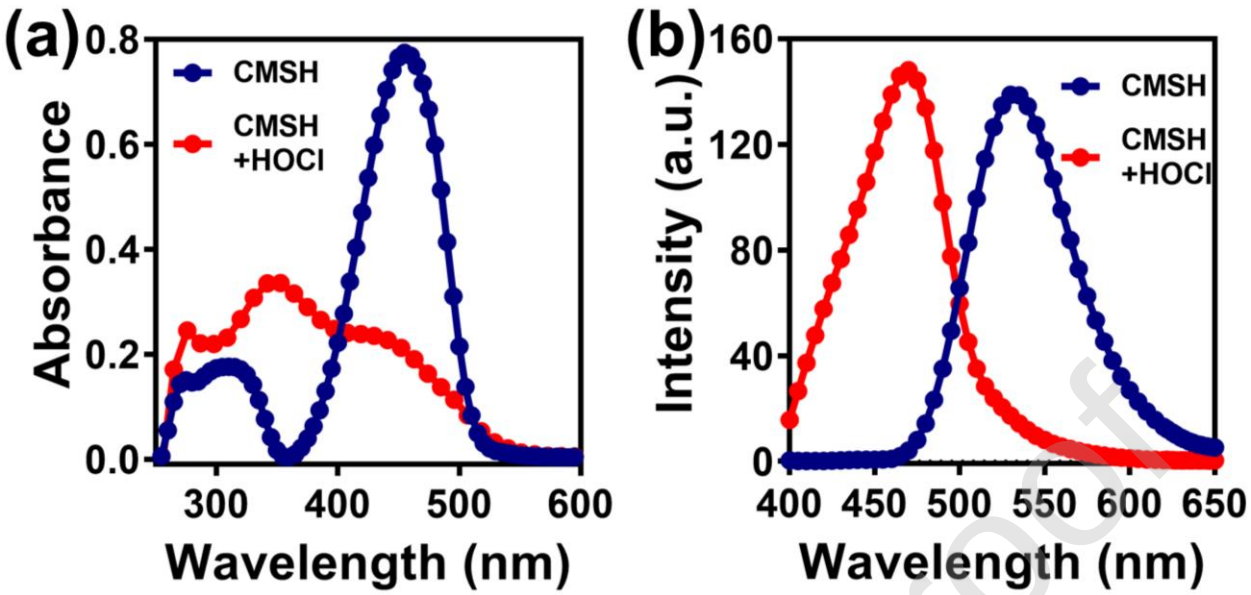

Fig. S5 (a) UV-vis absorption and (b) fluorescence spectra changes of 5 μM **CMSH** in EtOH/H_2O solution (v/v = 1/19) in the absence and presence of ClO^- (80 μM). Each spectrum was recorded after 5 min.

Table S1 Comparison of ratiometric fluorescent probes for ClO^-.

Probe structures	λex λem(nm)	Reagents	Detection limit/nM	Response time/s	Application
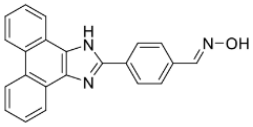	349 439 509	pH 9.0 PBS (80% DMF)	--	Within seconds	--
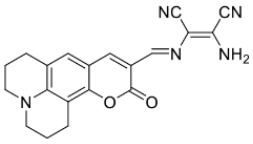	464 505 585	pH 7.4 PBS (20% DMF)	200	< 600	MCF-7 cells (Ex) Ex = exogenous
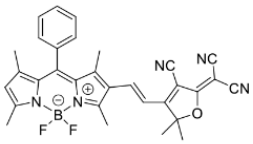	465 520 629	pH 7.4 PBS (1% EtOH, 0.1 % Triton X-100)	500	-400	RAW 264.7 cells (Ex, En) En= endogenous
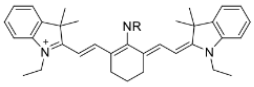	540 566 780	pH 7.4 PBS (0.5% DMF)	19.5	-360	HcLa cells (Ex)
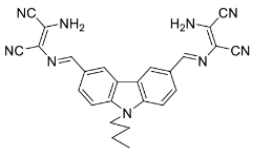	344 375 495	pH 7.4 HEPES (50% EtOH)	350	--	Water samples
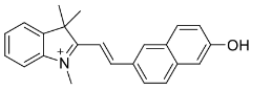	460 488 631	pH 7.4 PBS (75% THF)	93	-20	Water samples RAW 264.7 cells (En)
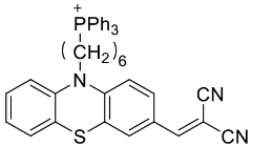	410 522 640	pH 7.3 PBS (0.5%DMS, 1 mM Triton X-100)	430	Few seconds	RAW 264.7 cells (En) Nude mouse (En)
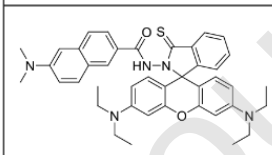	350 440 585	pH 6.0 PBS (30% EtOH)	100	< 50	RAW 264.7 cells (En)
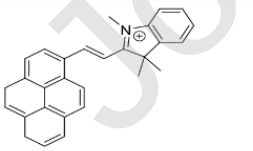	430 470 613	pH 7.4 PBS (5% DMSO)	350	4200	Water samples HeLa cells (Ex) RAW 264.7 cells (En)
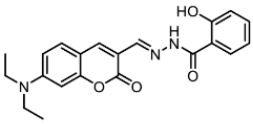 **(This work)**	**390 470 532**	**H_2O (5% EtOH)**	**128**	**< 40**	**MRC-5 (Ex) *E. coli* (Ex) Zebrafish (Ex) Test paper**

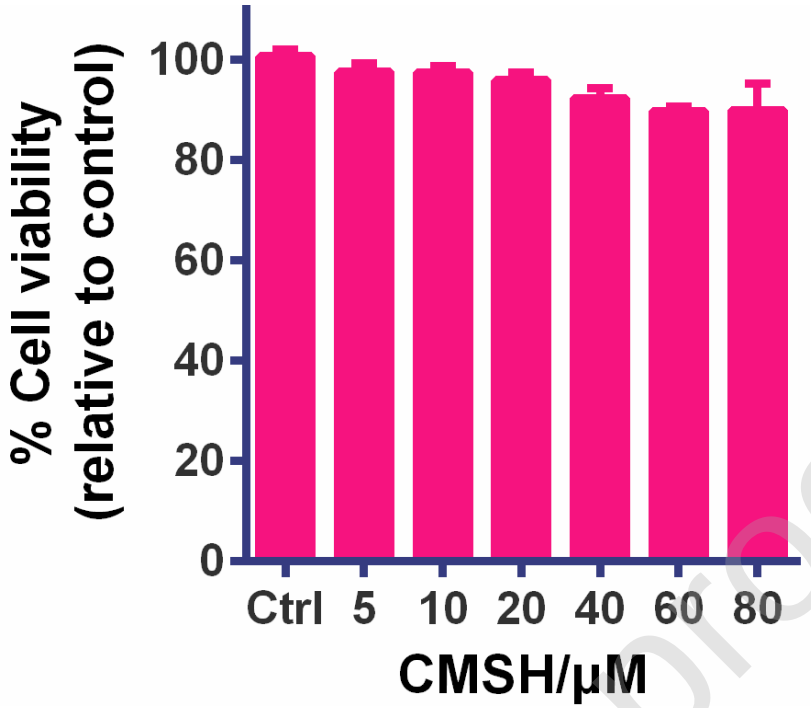

Fig. S6 Evaluation of the cell viability using the MTT assay in MRC-5 cells at 24 h. PBS treatment as a control group. The concentration of **CMSH** probe varied from 5 to 80 μM. Results are presented as the mean of the three measurements ± standard deviation. (n = 3)

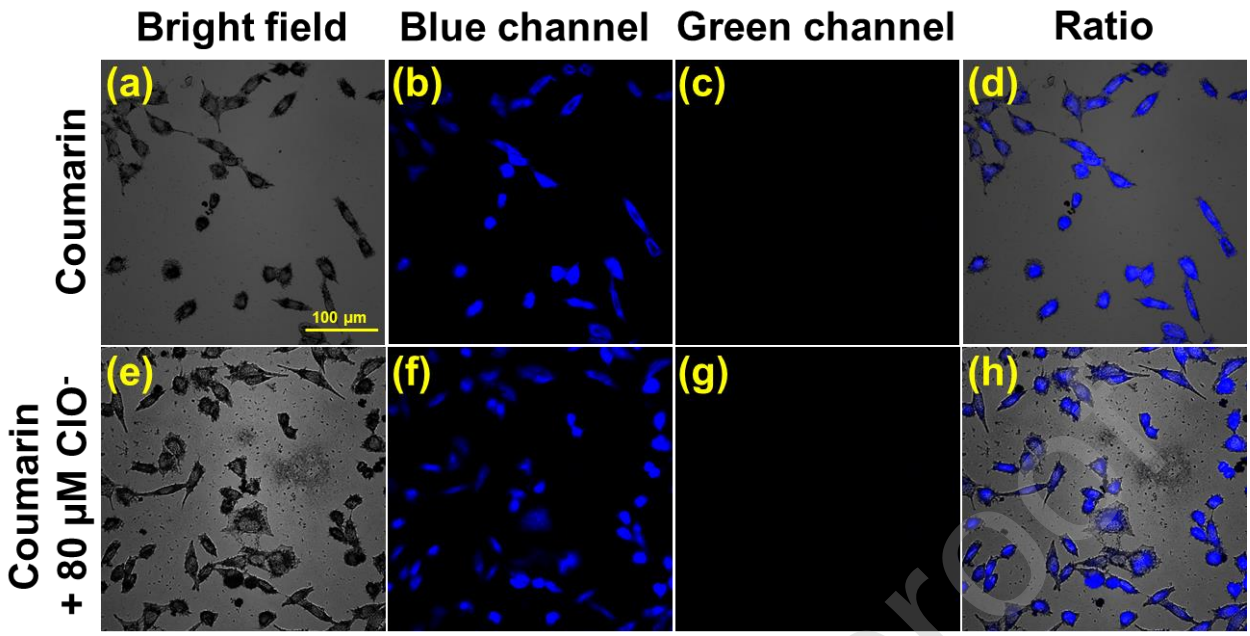

Fig. S7 Relative confocal fluorescence images of MRC-5 cells under different conditions with coumarin. MRC-5 cells treated with 5 μM coumarin (a-d), then further incubated with 80 μM ClO^- (e-h). Fluorescence images from left to right: blue channel, green channel and ratiometric images (Fblue/Fgreen).

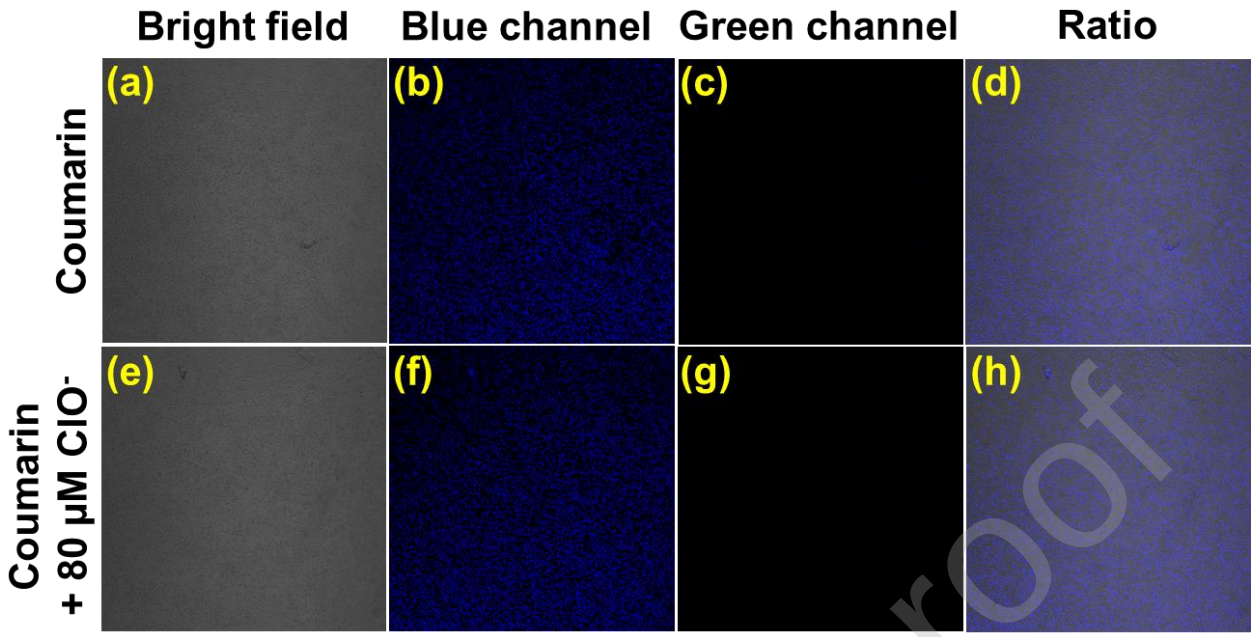

Fig. S8 Confocal fluorescence images of *E. coli*. Fluorescent image of *E. coli* stained with coumarin (5 μM) for 20 min (a-d). *E. coli* were incubated with coumarin for 20 min, further incubated with 80 μM ClO^- (e-h).

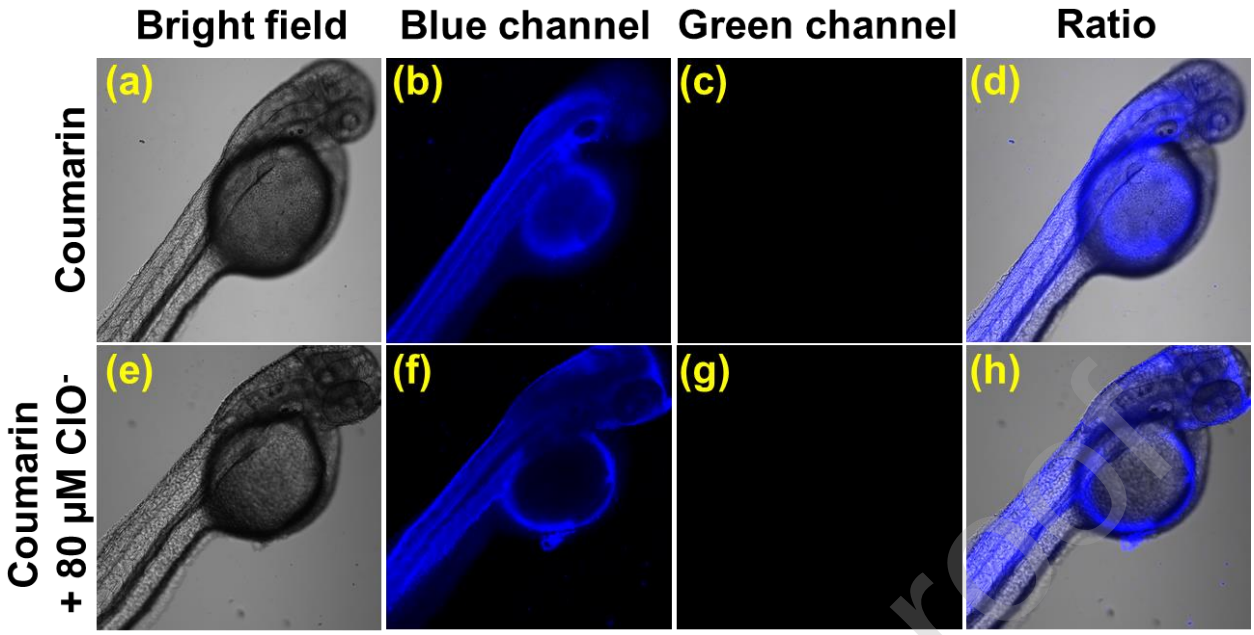

Fig. S9 Confocal fluorescence images of zebrafish. Fluorescent image of zebrafish stained with coumarin (5 μM) for 20 min (a-d). Zebrafish were incubated with coumarin for 20 min, further incubated with 80 μM ClO^- (e-h).